CHARACTERIZATION OF DESIGNED NOVEL CYTOCHROME P450 FOR INDUSTRIAL BIOCATALYSIS

A Thesis Submitted to
The Graduate School of Engineering and Sciences of
İzmir Institute of Technology
in Partial Fulfillment of the Requirements for the Degree of

MASTER OF SCIENCE

in Biotechnology

by
Tuğçe SAKALLI

December 2020
İZMİR

ACKNOWLEDGMENTS

First of all, I would like to thank my dear advisor Assoc. Prof. Nur Başak Sürmeli Eraltuğ who supported me, guided me and helped to expand my horizons during my graduate studies. She has always helped me in my higher education and provided all kinds of resources. I am really lucky to know and work with a valuable advisor like her.

I would like to present the Scientific and Technological Research Council of Turkey (TUBITAK) for supporting (116Z380) project.

Also, I would like to thank Prof. Dr. Hüseyin Çağlar Karakaya and Assoc. Prof. Dr. Ali Oğuz Büyükkileci for allowing me to use their laboratory during this study.

Furthermore, I would like give thanks my laboratory mates; Ekin Kestevur Doğru, Muhammet Semih Başlar, Gülce Güralp, Merve Erdal, Alper Şahin and Gamze Gürerk for everything. I would like to thank my office mates; Gülten Kuru, Eyüp Bilgi, Betül Karakuzu, Gamze Doğan, Öykü Sarıgil and Yiğit Ege Çömlekçi for their supporting and friendship.

Most importantly, I am thankful my best friends Yağmur Ceren Ünal, Buse Şirin, Damla Yüksel, , Gizem Tuğçe Ulu and Mine Kocabıyık for heartsomely and believingly.

Last but not least, I present thankfulness to my family very much for trusting and supporting me on this way.

ABSTRACT

CHARACTERIZATION OF DESIGNED NOVEL CYTOCHROME P450 FOR INDUSTRIAL BIOCATALYSIS

Biocatalysts are increasingly applied in chemical synthesis due to their high level of regioselectivity and enantioselectivity. P450s are important biocatalysts due to their ability to hydroxylate unactivated carbon atoms using molecular oxygen. P450s catalyze monooxygenation reactions by using nicotinamide adenine dinucleotide (phosphate) (NAD(P)H) as electron donor and electron transfer proteins. P450s can also utilize hydrogen peroxide (H_2O_2) instead of NAD(P)H and redox partners through a H_2O_2-shunt pathway. However, P450s are inefficient in oxygenation reactions with H_2O_2. Thermophilic enzymes demonstrates high stability at different temperatures, pH and organic solvents, so it is expected to increase implementations of enzymes. CYP119 is an acidothermophilic P450 from *Sulfolobus acidocaldarius*. In our laboratories, directed evolution was used to create improved mutants of CYP119 with higher oxidation activity when using H_2O_2. T213R/T214I CYP119 was such a variant. The aim of the study is investigations of T213R/T214I CYP119 whether it is a stable and efficient biocatalyst for selective oxidation of hydrocarbons, which does not require expensive cofactors and electron transfer proteins or not. T213R/T214I CYP119 was expressed and isolated under optimized conditions. Peroxidase activity of T213R/T214I CYP119 was tested and compared to wild type (WT) CYP119. Characterization of T213R/T214I CYP119 shows higher peroxidation activity of enzyme for Amplex® Red, guaiacol and ABTS and epoxidation of enzyme for styrene substrates compared to CYP119. T213R/T214I CYP119 have higher affinity for progesterone and lower affinity for lauric acid. Mutations on Thr213 and Thr214 residues the active site will shed light on the design of novel CYP119 mutants in the future.

ÖZET

ENDÜSTRİYEL BİYOKATALİZ İÇİN TASARLANMIŞ YENİ SİTOKROM P450'NİN KARAKTERİZASYONU

Biyokatalizörlerin yüksek seviyeli enantiyo ve bölge seçiciliği sayesinde kimyasal sentezinde kullanım alanları artmıştır. P450'ler, moleküler oksijeni kullanarak aktifleştirilmemiş karbon atomlarını hidroksile etme yeteneklerinden dolayı önemli biyokatalizörlerdir. P450'ler electron donorü ve electron transfer proteinleri olarak nikotinamid dinucleotide (fosfat) (NAD(P)H) kullanarak monooksijenasyon reaksiyonlarını katalize etmektedir. P450'ler ayrıca NAD(P)H yerine hidrojen peroksit (H_2O_2) ve bir H_2O_2-şant yolu aracılığıyla redoks partnerleri kullanabilmektedir. Bununla birlikte, P450 enzimleri, H_2O_2 ile oksijenasyon reaksiyonlarında verimsizdir. Termofilik enzimler, farklı pH, yüksek sıcaklık ve organik solüsyonlara karşı yüksek stabilite göstermektedir. Bu sebeple geniş bir kullanım alanı olması beklenmektedir. CYP119 *Sulfolobus acidocaldarius*'dan elde edilen asidotermofilik P450'dir. Laboratuvarımızda yönlendirilmiş evrim ile H_2O_2 eşliğinde yüksek oksidasyon aktivitesi gösteren CYP119 mutantlarının tespiti için mutant kütüphaneleri oluşturulmuştur. T213R/T214I CYP119'u bu kütüphaneden elde edilen en yüksek aktivite gösteren mutanttır. Bu çalışmanın amacı, T213R/T214I CYP119'un pahalı kofaktörler ve elektron transfer proteinleri gerektirmeyen hidrokarbonların seçici oksidasyonu için kararlı ve verimli bir biyokatalizör olup olmadığının araştırılmasıdır. Ayrıca yüksek oksijenleme aktivitesine sahip olan bu mutantın farklı substrat ile etkileşimleri , peroksidasyon, epoksidasyon reaksiyonları ve sıcaklık ve aktivite ilişkisi ve organik solventlere karşı duyarlılılığı gibi birçok açıdan karakterize edilmesi ve WT CYP119 ile karşılaştırılarak farklı yönlerinin açığa çıkarılması hedeflenmektedir. T213R/T214I CYP119'un karakterizasyonu, CYP119'a kıyasla Amplex® Red, guaiacol ve ABTS ve stiren için enzimin daha yüksek peroksidasyon ve epoksidayon göstermektedir. T213R/T214I CYP119, progesteron için daha yüksek afiniteye ve laurik asit için daha düşük afiniteye sahiptir. Enzimin aktif bölgesindeki Thr213 ve Thr214 kalıntılarındaki mutasyonlar, gelecekte yeni CYP119 mutantlarının tasarımına ışık tutacaktır.

TABLE OF CONTENTS

LIST OF FIGURES

Figure **Page**

Figure **Page**

LIST OF TABLES

Table **Page**

CHAPTER 1

INTRODUCTION

1.1. Biocatalysis and Biocatalyst

Enzymes are biological catalysts and are known as important stones of life. Enzymes supply metabolic requirements of cells and take role for maintaining life in biochemical reactions. Most of the natural enzymes demonstrate highly efficient and increased rates of biotransformation.

Enzymes can change the mechanism of a reaction that leads to an increase in the rate of the chemical reaction. Furthermore, significant features of enzymes are selectivity, reusability and high specificity. They catalyze a particular substrate or a group of substrates and recognize specific bond or linkage and a particular isomer [1]. Therefore, enzymes are used as biocatalysts in a wide range of industrial applications. For example; food processing, cosmetics, pharmaceutical and biotechnology etc.[2]

Biocatalysis is a type of chemical process that speeds up chemical reaction with the use of natural substances. Biocatalysis is a very common application used in many areas such as synthesis of chemicals and pharmaceutical industry. The most important feature of biocatalyst to perform reactions that are troublesome to carry out by chemical catalysts. Biocatalysts are known as environmentally friendly. Also, a fine biocatalyst should demonstrate high activity, specificity, efficiency.[3,4]

1.2. Protein Engineering

Proteins are important compounds in biological life. Proteins, enzymes, realize many biochemical reactions as biocatalysts in cells. For example, macromolecule synthesis, energy conversion, reproduction etc. that take place in a cell.

Important features of enzymes are selectivity, reusability and high specificity. Enzymes are used as biocatalysts in a wide range of industrial applications. For example, food processing, cosmetics, pharmaceutical and biotechnology etc. In the modern biotechnology, enzyme engineering approaches has been used widely in pharmaceutical

industry Because, enzymes engineering approaches have enabled the development of enzymes that can catalyze novel small molecule transformations that may be difficult or impossible using classical synthetic organic chemistry[5–7]. Design of enzymes results in an increase of specificity of the enzyme and increases the kinds modifications that can be catalyzed by the enzyme in research laboratories [8] Combination of protein engineering technologies provides information to create novel enzymes for using in new biotechnological and industrial applications. Because specificity and selectivity of enzymes are altered for desired kinetic and thermodynamic features and increased substrate diversity [9]

Protein engineering is a very common application. It has an advantage for creating special biocatalyst with required functions in pharmaceutical and agrochemical industry. Biocatalysts have been developed for increased of stability, thermodynamic features, and by protein engineering. There are three main approaches for protein engineering. These are directed evolution, rational and combinatorial design [10,11]. Some protein engineering techniques have been discussed in the following section.

1.2.1 Rational Design

Rational design technique is used for protein engineering if protein structure is known or possible to predict with different approaches. Because rational design requires some information about enzymes such as function, active site of enzyme etc. On the other hand, this technique is easy and cheaper. When enzymes are designed by rational approaches, production process can be easily done with site directed mutagenesis

1.2.2 Directed Evolution

Directed evolution is a type of protein engineering technique that is inspired from natural evolution. Random genetic mutations are applied to the genetic code of the enzyme[12,13]. Error-prone PCR, staggered extension process and DNA shuffling are methods used for directed evolution. Directed evolution technique does not need any information about function of enzymes or three-dimensional structure of enzyme. Furthermore, it does not require knowledge of mutation effect on the enzyme structure or function. The first step of directed evolution is random mutagenesis and then molecular

diversity can be increased by *in vitro* recombination techniques. Improved desired phenotypes are selected by high-throughput screening[1]. However, this application has problems due to the limited dataset of protein libraries [1].

Novel biocatalysts are improved depending on increased catalytic activity, substrate specificity and stability by directed evolution. However, directed evolution needs a high throughput screening method for selection of mutants with desired features. Screening method should be simple, fast, efficient, and cost effective so that enzyme activity can be measured with a microtiter plate. Cost-effective screening methods are developed for many cytochrome P450s (P450s) by using fluorescent substrates, products with different peroxides [14].

There are differences between rational design and directed evolution method. Rational design is used for protein engineering if protein structure is known or possible to predict with different approaches. Mutation on native enzyme was created as computationally. Created mutants were obtained by site directed mutagenesis. On the other hand, native enzyme was mutated by random mutagenesis in the directed evolution. Large mutant library was obtained. Large mutant library is screened and selected. was performed. Rational design and directed evolution techniques were illustrated in Figure1.1.

1.2.3 Semi Rational Design

Semi rational design occurs through a combination of directed evolution and rational protein design. Since, there are limitations for both directed evolution and rational protein design. This combined technique is called semi-rational design[15]. Structure and function of protein is known in the semi-rational design approach. Therefore, small but rich library can be created based on this information. This technique gathers all the information available through computation modeling/bioinformatics approaches to identify the most promising target site with a small diversity in amino acid for protein engineering. Semi-Rational design helps creation of a good biocatalyst which has high selectivity, stability, wide-range substrate with the help of bioinformatic applications [9]

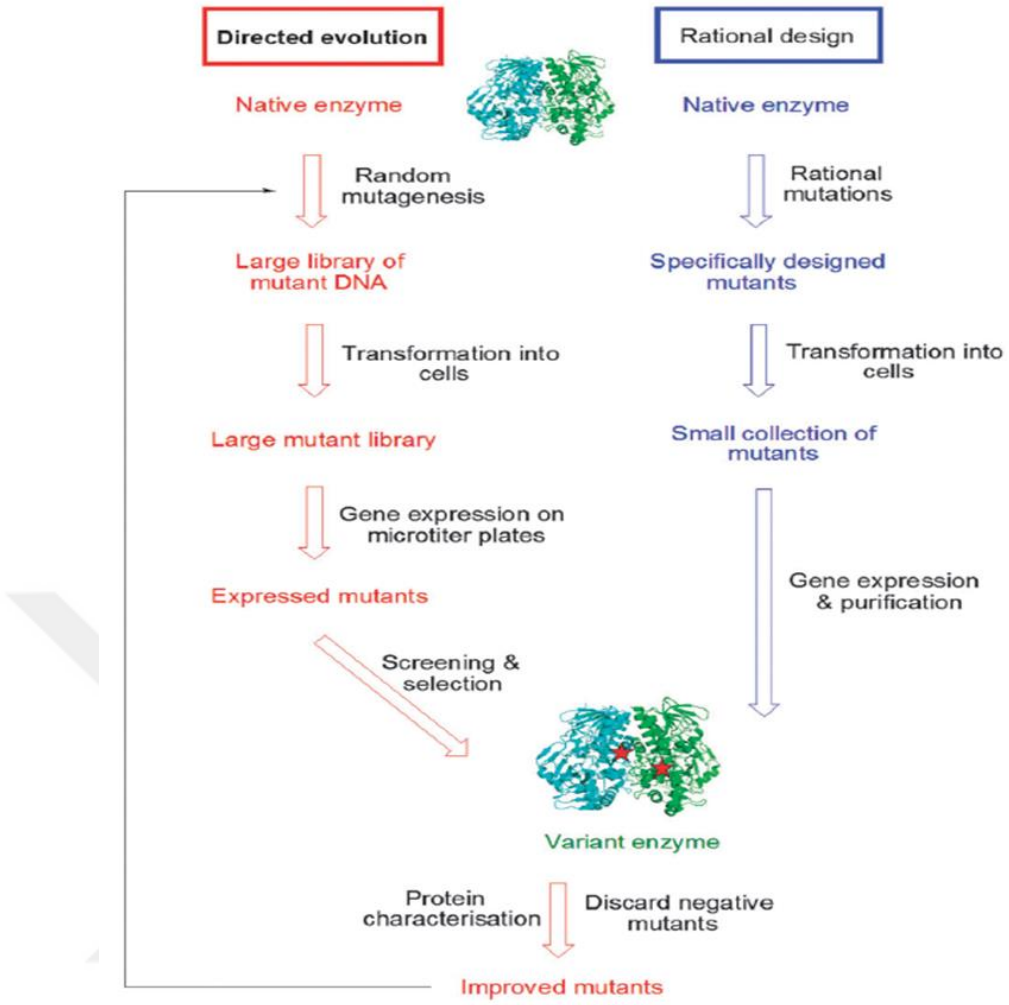

Figure 1.1 Differences were demonstrated between directed evolution and rational design[9]

1.3. Cytochrome P450s (P450s)

P450s are one of the largest families of enzymes found in all classes of life. P450s are involved in the realization of a wide range of biochemical reactions[16]. P450 enzymes are monooxygenase enzymes that catalyze monooxygenation reactions with high regio and stereoselectivity[17,18]. The most common reaction of P450 monooxygenases catalyze cleavage of bound molecular oxygen and formation of an oxygenated product atom of a substrate [19].

P450s contain the heme prosthetic group, that is important for enzymatic activity. The heme cofactor in P450s consists of iron ion bound to the protoporphyrin IX. The

ferric ion is coordinated by the nitrogen atoms of the protoporphyrin ring as shown in Figure 1.2 and plays an important role in catalysis.

There are two oxidation states of the heme iron atom; Fe^{2+} (reduced, ferrous) and Fe^{3+} (oxidized, ferric) in protoporphyrin IX. The heme group is bound to a single polypeptide chain by the thiol group of a conserved cysteine amino acid (Figure 1.2B)[20,21]. Protoporphyrin IX is linked to the cysteine residue that is placed near to the C-terminus of the polypeptide chain as noncovalently. In the catalysis of the microsomal P450 enzymes, two electrons come from the cofactor NADPH. These electrons are transported from NADPH by the flavoprotein reductase to the P450 heme group. A water molecule is located at the sixth coordination site of the heme iron. During the catalytic cycle, the water molecule is displaced by the molecular oxygen [22]

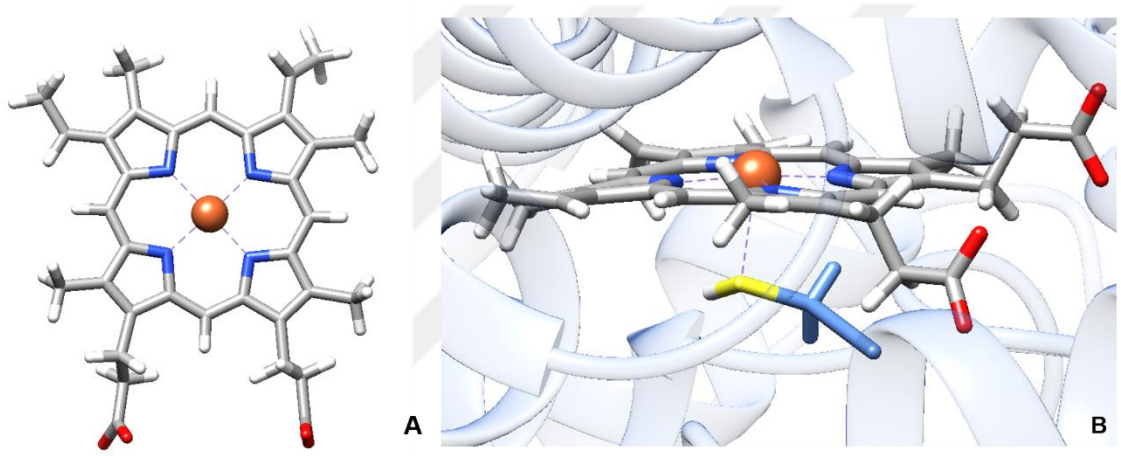

Figure 1.2 Image of heme group of P450s were created with UCSF Chimera (PDB ID: 1F4T). Heme involves four nitrogen atoms (blue) and Protoporphyrin IX ring (gray) (A). Heme group is tethered to protein via thiol group (yellow) of conserved cysteine residue (blue) (B).

P450s can catalyze many reactions with a variety of substrates including hydroxylation dealkylation, epoxidation, and sulfoxidation. P450s become more popular industrial production of reward chemicals. Besides these reactions, P450 enzymes have been used as dehydrases, reductases and isomerases [23,24].

On the other hand, performing oxidation reactions by P450s require electron transfer proteins and expensive cofactors (NAD(P)H) [25]. If hydrogen peroxide (H_2O_2) can be utilized as an oxidant in P450 reactions, the reductase proteins are not necessary. However, H_2O_2 cannot be used at high concentrations for whole cell catalysis. Another negative factor is that most eukaryotic P450s do not have high solubility. These features cause limitation in the application of P450s in the industry[26]. In contrast, bacterial P450s

are more favorable for uses of industrial applications, since bacterial P450s are soluble in contrast with eukaryotic P450s which are membrane bounded and not soluble [27]. Furthermore, P450s demonstrate small sequence similarity, but the three-dimensional structure of enzymes are similar. As all P450s have the similar three-dimensional structure, it can be thought structurally related residues indicate equal function in the enzyme.

P450s are separated into two classes which are Class I and Class II based on the type of their redox partner. Ferredoxin/ferrodoxin reductase system is used by Class I enzymes as electron donor for prokaryote while NADH/NADPH reductase system is accepted electrons by Class II enzymes for eukaryote[28]. Also, P450s include many minor classes[29]. P450s fused to their diflavin reductase partner in one polypeptide chain e g , P450BM3. One component enzyme uses NADPH-dependent, FMN-containing reductase and ferredoxin which are attached to the heme domain of P450s.

Catalytic cycle of P450s is illustrated in Figure 1.3. First, the substrate binds to the enzyme. Two electrons come from NAD(P)H and one of them converts ferric heme iron (Fe^{+3}) ion into ferrous form (Fe^{+2}). Then, ferrous heme bind to molecular oxygen. After the transfer of the second electron, ferric-peroxy species are formed. Afterwards, protonation of ferric-peroxy intermediate result in cleavage of molecular oxygen so a water molecule and oxyferryl radical cation (Compound I) is formed. Oxyferryl radical cation is known as the major oxidation agent in P450 oxygenation reactions. Finally, oxyferryl species attack the substrate which is bound. Therefore, substrate is oxygenated and ROH product is formed. Instead of molecular oxygen, hydrogen peroxide (H_2O_2) can take the role of the oxidant and electron donor that is called peroxide shunt pathway. Peroxide shunt pathway is not efficient for most of P450s. However, previous studies have shown that in some cases H_2O_2 have been utilized instead of the natural redox partner-driven systems[30]. CYP1A2 is given as example of H_2O_2 oxidation. CYP1A2 catalyze oxidation of a heterocyclic amine by using H_2O_2. CYP3A4 and CYP2D6 could change from the cyano group of drugs pinacidil to the suitable amide in the presence of H_2O_2 [31]. If large scale of oxidized product is necessary, the hydrogen peroxide shunt pathway is not used due to insufficient yields of product obtained. The reason of low product formation is that heme prosthetic group and active site amino acids are altered by oxidative modification[30].

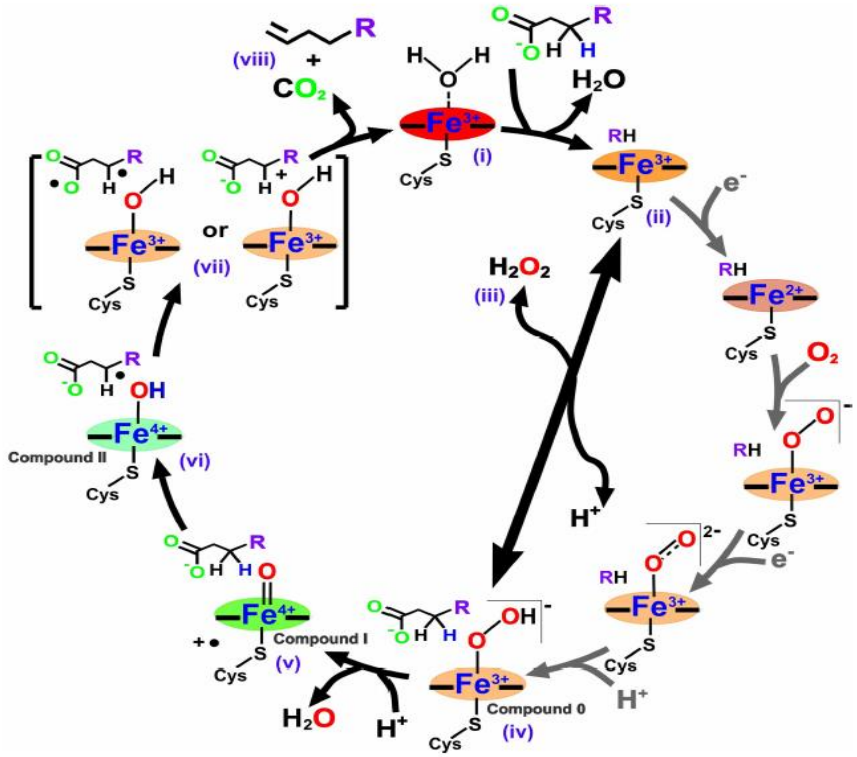

Figure 1.3 P450 catalytic cycle [30]

1.4. Stability of P450s

Use of P450s is limited because of instability in industrial conditions. Especially, P450s are not stable under the condition when they fall into isolation, storage and use. Recent studies have concentrated on different factors for increased stability of P450s. On the other hand, thermal stability is the most important factor that limits use of P450s in industrial applications, but some of the enzymes do not disrupt structure at high temperatures[9]. Because hyperthermophiles live between 80º C and 100º C [32]. Enzymes of hyperthermophiles are examined to study thermostability. Some residues on thermostable enzymes control to preserve thermostability. *Sulfolobus acidocaldorius* is one of the thermophilic enzymes in P450 families[17,33]. The thermophilic enzyme structure is solved. Aromatic clusters are found in this enzyme but mesophilic P450s do not have. In this way, this difference is used to design thermostable enzymes. Arnold and coworkers increase thermostability of P450 BM3 enzymes which show peroxygenase activity. The creation of P450 BM3 displays thermostability and peroxygenase activity without using NADPH and redox partners. However, it does not stable after isolation [34,35].

On the other hand, Aromatic clustering has an important role in increasing the thermal stability of CYP119. However, aromatic clustering does not have only one factor that affects the thermal stability of the P450s. Although CYP175A1 is a thermophilic enzyme , it does not contain an aromatic cluster. The 26 residues of CYP175A1 include 8 salts bridges. Salt bridge has an effect on thermal stability of the enzyme [36].

1.5. Solvent Tolerance in P450 enzymes

Water is important solvent in our life. However, it is weak solvent for many synthetic reactions. Organic solvents are generally needed to increase the solubility of hydrophobic substrates and change the thermodynamic equilibrium to favor synthesis ,but solvent stability is one of the limitations to the utilize of enzymes in industrial biotechnology. Generally, enzymes are not stable enough under processing conditions. However, use of the organic solvents in the enzymatic reaction offers many advantages. For example, solubility of hydrophobic substrates increases. Also, water dependent side reactions were prevented by using of organic solvents [37]

Many studies have shown that P450s are not stable in the presence of organic solvents. Also, small amounts of organic solvents can inhibit activity of P450s. Increased stability of P450s for organic solvents are examined by many approaches. P450 BM3 has been designed to show raised stability in a number of organic solvent [99] On the other hand, thermophilic CYP119 demonstrates resistance to organic solvents so that the CYP119 can be used to catalyze various substrates.

1.6. CYP119

CYP119 is a thermophilic enzyme that belongs to the P450 family. CYP119 was isolated from *Sulfolobus acidocaldorius* that is an acidothermophilic bacteria. *Sulfolobus acidocaldorius* is known as sulfur- oxidizing organism [2,23]. These organisms can live in extreme conditions such as pH 2.4 and temperature 83º C [38,39]. When CYP119 and P450cam which is mesophilic enzyme are compared to each other, CYP119 melts at 90º C but P450cam melts at 50º C. [40].The heme binding region of CYPs is highly conserved among P450 families. In CYP119 (366 amino acids), the N-terminal segment and surface loop are shorter than other CYPs (400-450 amino acids). P450s are observed in many organisms so that it is not surprising that they are observed in thermophiles. The structure

of CYP119 was analyzed by Yano and coworkers[41]Afterwards, independent structures of CYP119 were determined by Park and coworkers [42]

Crystal structure of CYP119 is shown in the Figure 1.4. Though natural substrates of CYP119 are not known, CYP119 takes role in many reactions such as peroxidation, hydroxylation, oxidation and dehalogenation. CYP119 contains an aromatic clustering which takes role thermal stability of the enzyme. For example, when the Phe24 residue that is located in the aromatic cluster of CYP119 is converted to Ser by the mutation, the melting temperature decreased for about 10ºC [41,42]

In CYP119 Thr213 is located in the heme active site; it takes role in the catalytic activity. Iron spin state is controlled in part byThr214. According to topological analysis with aryldiazenes, Thr213 is also close to iron atom of the heme and located to above pyrrole rings A and B. In contrast, Thr214 is a little distance away. Putidaredoxin and putidaredoxin reductase reduce the CYP119 slowly. Thr213 and Thr214 residues on the active site do not take role in thermal stability since their mutation did not significantly alter the melting temperature . CYP119 does not include a hydrophobic tail so it is soluble. CYP119 shows high identity in the heme binding region with mammalian, fungal and bacterial CYPs. CYP119 shows 33% high identity with $P450_{eryF}$ (CYP107A1). P450eryF take role the biosynthesis of erythromycin Like all P450s CYP119 contains the conserved Cys317 that covalently binds to the heme iron and highly conserved threonine in the helix I. Conserved threonine may play a role in the coordination of a water ligand to the ferric heme. Also, Thr214 plays a role in oxygen binding to ferrous prosthetic groups and then, the bound dioxygen is cleaved, and the final activated oxidizing species is formed. P450 enzymes can convert from low spin to high spin state. This conversion of the P450s are monitored by the shift between 415 and 390 nm in Soret absorbance which is related loss of the distal water [43,44]Temperature, pH and ionic strength change spin state of P450s. CYP119 has conserved Thr213, Thr214 that are unique for CYP119 compare to CYP119[39]. Threonine residues in CYP119 take role controlling catalytic activity, spin state and structure of active site [2]

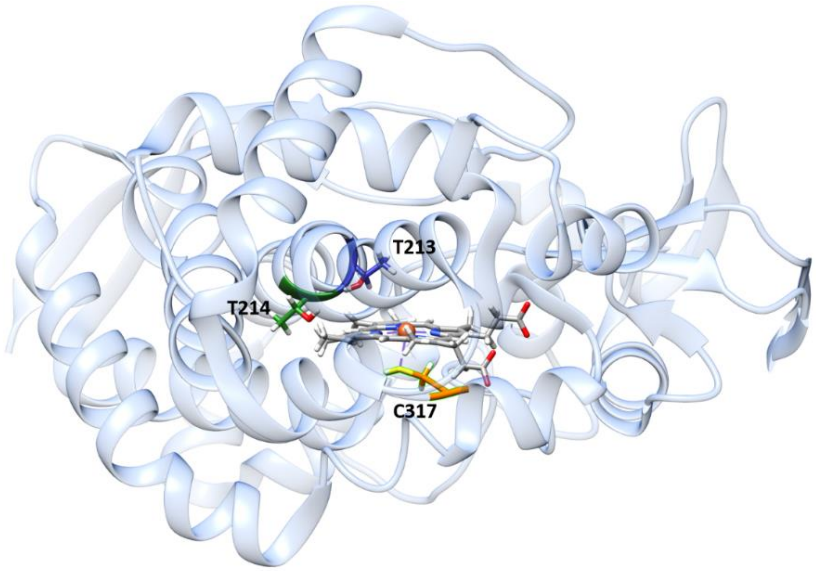

Figure 1.4 Structure CYP119 (PDB:1F4T) were created by UCSF Chimera. Thr213(blue), Thr214(green) , Cys317 (yellow and orange) and were marked.

1.7. Major Reactions Catalyzed by P450 Monooxygenases

More than 20 reaction types are catalyzed by P450 monooxygenases. Unactivated-sp3-hybridized C atoms are hydroxylated by P450s. Hydroxylation reaction is classical reaction of P450s. For example, hydroxylation of saturated fatty acids is performed by eukaryotic CYP4A3 and bacterial CYP102 (e.g. P450BM-3) enzymes[45,46].

P450s can catalyze cleavage of bound molecular oxygen and formation of an oxygenated product.

Most common reaction of P450s is shown in equation 1:

$$\textbf{Equation 1: } RH + O_2 + 2e^- + 2H \longrightarrow ROH + H_2O \qquad (1)$$

This is known as monooxygenase activity. In this activity, P450s use H_2O_2 and cumene hydroperoxide and other peroxides as oxygen donors for oxygenation of substrates. CYP monooxygenases can take role in peroxidases.

1.7.1 Peroxidation Reaction catalyzed by Cytochrome P450

Some of P450s utilizes H_2O_2 and other peroxides and they catalyze one electron oxidation of substrate. An significant reductive activity of P450 which is peroxidase function was discovered by Hrycay and coworkers. Peroxidase function of P450s causes that hemoprotein decreases and detoxifies biological hydroperoxides such as hydrogen peroxide. This function of P450s illustrates that it has catalytic versatility[47]. Archaeal CYP119A1 from *Sulfolobus acidocaldarius* can catalyze the peroxygenation of laurate and styrene in the presence of H_2O_2 and other peroxy compounds[22]. Some of peroxidation and oxidation reactions were explained next part.

1.7.1.1 Amplex® Red Peroxidation Reaction

Amplex® Red (*N*-acetyl-3,7-dihydroxyphenoxazine) is a colorless substrate that can be oxidized in the presence of H_2O_2 by peroxidase. Resorufin which is a red fluorescent compound is formed by oxidation of Amplex® Red (excitation/emission maxima=571/585 nm). Amplex® Red peroxidation by H_2O_2 was catalyzed withCYP119 (Figure 1.5). Also, H_2O_2 concentration can be determined by using Amplex® Red as a probe with horseradish peroxidase (HRP) [48,49]. Previously, Amplex® Red has not been utilized as screening methods for P450s using cell lysates. However, the screening method of Amplex® Red was optimized to use for determination of peroxidation activity of CYP119 in our laboratories.[50]Amplex® Red Peroxidation reaction is illustrated in Figure 1.5.

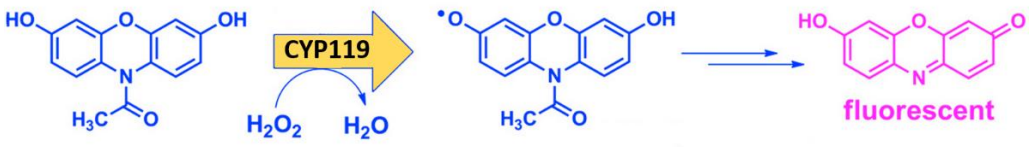

Figure 1.5 Amplex® Red peroxidation reaction in the presence of H_2O_2 is illustrated.

1.7.1.2 Guaiacol Oxidation Reaction

Heme-containing proteins such as guaiacol peroxidase oxidize aromatic electron donors in the presence of H_2O_2 [51]. The peroxide is rapidly transformed to water and oxygen in the presence of peroxidase. Brown product is formed, which is tetraguaiacol, due to oxidation of guaiacol. Brown color product is measured by using

spectrophotometer[52].The peroxidase enzymes catalyze oxidation of guaiacol (a colorless liquid) in the presence of H_2O_2.[52].

The peroxidase enzymes catalyze guaiacol in the presence of H_2O_2. Tetraguaiacol (a brownish color) is formed at the end of the reaction and water in the presence of peroxide. Assay product has a maximum absorption around 470 nm[53]. The peroxidation reaction of peroxidase enzyme are shown in the following Figure 1.6:

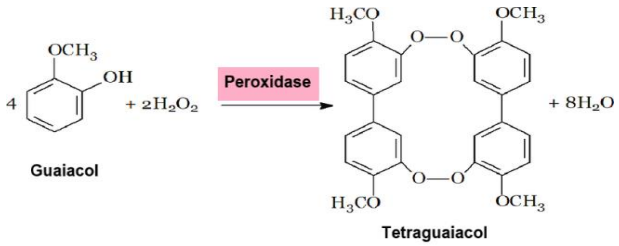

Figure 1.6 Guaiacol peroxidation reaction in the presence of H_2O_2 was drawn.

1.7.1.3 ABTS Oxidation Reaction

ABTS (2,2'-azino-bis(3-ethylbenzothiazoline-6-sulfonic acid)) is a compound that is used for determination of reaction kinetics of specific enzymes. ABTS is generally used in enzyme-linked immunosorbent assay (ELISA). Because binding molecule of molecules was detected in the presence of ABTS.

On the other hand, peroxidase such as HRP catalyze ABTS oxidation catalyzed by peroxidase in the presence of H_2O_2. ABTS is green color. and soluble product. Product of ABTS oxidation is $ABTS^{\bullet+}$ radical cation. $ABTS^{\bullet+}$ radical cation formation can be followed by absorbance at 734 nm in UV spectrophotometer [54].

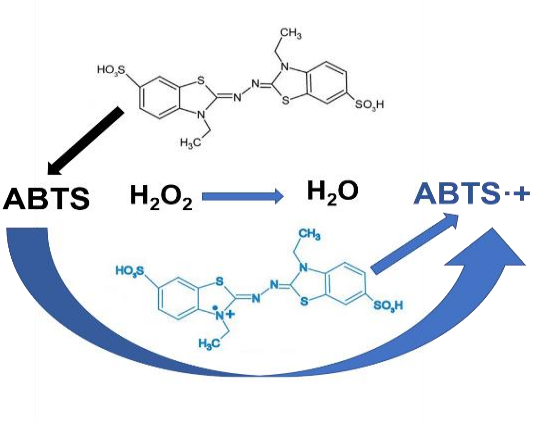

Figure 1.7 ABTS peroxidation reaction was illustrated

1.8. Scope of This Study

The goal of this thesis is characterization of an improved novel mutant of CYP119, T213R/T214I CYP119, which was obtained from screening of Amplex® Red peroxidation activity assay. T213R/T214I CYP119 was selected from a high throughput screening library because it shows enhanced peroxidation using H_2O_2 as an electron donor and an oxidant[50]. For most P450s NAD(P)H is used as electron donor, but it is an expensive reagent for industry. On the other hand, most P450 enzymes do not use H_2O_2 efficiently in the peroxide shunt pathway. The novel T213R/T214I CYP119 was investigated in terms of peroxidation activity. In this study, peroxidation activity of T213R/T214I CYP119 was investigated in the presence of Amplex® Red, guaiacol and ABTS with H_2O_2 and was compared to WT CYP119. Stability of WT CYP119 and T213R/T214I were also investigated in terms of temperature, pH and organic solvents. Docking studies were performed to investigate if T213R/T214I mutations on the active site of CYP119 expands the substrate range of the enzyme.

CHAPTER 2

METHODOLOGY

2.1 Plasmid Isolation of T213R/T214I CYP119

Previously, CYP119 mutant library created by targeted random mutagenesis on Thr213 and Thr214 residues. The large CYP119 mutant library transformed into the *E.coli* BL21 (DE3) cells[50] Improvement of peroxidase activity of T213R/T214I CYP119 was obtained by screening of large CYP119 mutant library with Amplex® Red peroxidation activity assay. Improve T213R/T214I mutant of CYP119 was stored in glycerol stocks at -80° C. Inoculation of the colony containing the improved variant (T213R/T214I CYP119) was performed from glycerol stock into the petri plate by streaking plate method. Petri LB agar plate with 0.1 mg/ml ampicilin was incubated at 37 °C during overnight. Four colonies picked from the petri plate randomly. The colony containing the improved mutantT213R/T214I CYP119 (pet11a vector +mutant CYP119) was grown in 5ml Lysogeny Broth (LB) (Duchefa Biochemie, LB Broth low salt;10 g/L tryptone, 5 g/L yeast extract and 10 g/L NaCl) with 0.1 mg/mL ampicillin. New glycerol stocks of T213R/T214I CYP119 were prepared for each colony by adding 500 µl glycerol into 500 µl *E.coli* culture in cryo tubes.

Sequence analysis was performed with four randomly selected colonies to check the presence of novel mutant. Four picked colonies were grown in 10 mL of Lysogeny Broth (LB) (Duchefa Biochemie, LB Broth low salt;10 g/L tryptone, 5 g/L yeast extract and 10 g/L NaCl) containing 100 µg/mL ampicillin at 37 °C with 220 rpm shaking overnight. After overnight of growth, plasmids were isolated by using Presto Mini Plasmid Kit (Geneaid, PDH100). *E.coli* cells were centrifuged at 3900 rpm for 15 mins. Supernatant was poured and pellet was dissolved in 200 µL of PD1 buffer containing RNase and suspension was put into a microcentrifuge tube. Cell lysis was initiated by adding 200 µL of PD2 buffer and inverting the tubes 10 times. After, tubes were waited 2 minutes at room temperature. 300 µL of neutralization buffer PD3 was put into tubes and mixed by turning the tubes up and down 10 times. These tubes were done centrifugation at 15,000 x g for 8 mins, then supernatants were taken. Supernatants were

loaded into PDH columns that have the 2 mL collection tubes. After loading, the columns were washed with 600 µL of wash buffer and centrifuged at 15,000 x g for 3.5 mins. After washing steps, columns were put into new tubes. Isolated plasmids were obtained by elution steps. 50 µl elution buffer was added into the columns. Microcentrifuge tubes that contain PDH columns were centrifuged at 15,000 x g for 2 mins.

Concentration of isolated plasmids were determined by using Thermo Fisher Scientific Multiskan GO (10680879) and µDrop Plate (Thermo Scientific, N12391). Plasmid concentrations were diluted to required concentrations for sequencing and sequence analysis was performed by Triogen.

2.2 Expression Test of T213R/T214I CYP119

Four randomly selected colonies of T213R/T214I CYP119 were indicated as colony 1 (C1), colony 2 (C2), colony 3 (C3) and colony (C4) were stored at -80ºC in glycerol stocks. C1, C2, C3 and C4 of glycerol stocks were inoculated into the 5mL LB medium with 0.1 mg/mL ampicillin. They were grown at 37ºC for 16 hours. After that, 80 µl of *E.coli* in LB medium was inoculated into 8 mL of 2xYT medium with 0.1 mg/mL ampicillin. Optical density (OD) was followed at 600 nm. After OD_{600nm} reached 0.7, 1 mM isopropyl ß-D-1- thiogalactopyranoside (IPTG) was added for induction of protein expression. Protein expression levels were checked by Sodium Dodecyl Sulfate-Polyacrylamide Gel Electrophoresis (SDS-PAGE) analysis.

2.3 SDS-PAGE Analysis

SDS-PAGE was utilized to analyze the success of CYP119 protein expression, isolation and purification. T213R/T214I bands were detected at corresponding molecular weight (~ 43 kDa). Samples were taken each isolation and purification steps of enzyme. These samples were mixed with loading dye (100 mM Tris-Cl, 4% SDS, 0.2% bromophenol blue and 20% glycerol) and 1 mM dithiothreitol (DTT). Then, SDS samples and protein ladder were heated at 90 °C for 3 minutes before loading into the gel. Samples and protein ladder were loaded into the gel and run at 30 Volt. After 1 hour, the gel was run at 90 volts. The SDS-PAGE was stopped, when the observe bands came to the end of the gel. The gel was stained with Coomassie Brilliant Blue dye and destained with a solution containing acetic acid and ethanol for bands to appear.

2.4 Production of WT CYP119 and T213R/T214I CYP119

Colony C4 was selected for large scale expression. Colony C4 was inoculated from glycerol stock into the 10 mL LB Broth with 0.1 mg/mL ampicillin. Culture was grown overnight in a shaking incubator at 220 rpm. 5 mL overnight culture inoculated to 500 ml 2xYT (16 g/L tryptone, 10 g/L yeast extract and 5 g/L NaCl at pH 6.8) medium with 0.1 mg/mL ampicillin and incubated at 37ºC by shaking at 220 rpm. When optical density (OD) reaches 0.7 at 600 nm, 1 mM IPTG was added into T213R/T214I CYP119 culture for induction of expression. They were expressed for 30 hours at 30ºC. After expression, cells were centrifuged at 3900 rpm for 30 minutes for harvesting. Then, obtained pellets were stored -80ºC.

2.5 Isolation and Purification of WT CYP119 and T213R/T214I CYP119

The frozen cell pellets of T213R/T214I CYP119 were dissolved with lysis buffer (150 mM NaCl, 10 mM imidazole, 0.2 mM phenylmethylsulfonylfluoride (PMSF), 1 mM benzamidine HCl, 50 mM potassium phosphate at pH 7.5). Sonication was applied on the cells for 30 s three times with 1 min intervals and then cell lysates were put on the water-bath at 60ºC for 1h. Centrifugation was applied to the cells 3900 rpm for 1.5 h at 4ºC for removal of precipitated proteins. Supernatants were taken and purified by ammonium sulphate precipitation. Firstly, 30% amount of ammonium sulphate was added slowly into the supernatant at the same time supernatant was mixed with stirrer on the ice. After addition of ammonium sulphate is finished, mixing of supernatant was continued for one hour. At the end of the one hour, supernatant was centrifuged at 3900 rpm for 45 min at 8º C for removal of precipitated protein. Supernatant was taken and put into the beaker. Ammonium sulphate amount is increased from 30% to 60%. Required amount of ammonium sulphate was added into the supernatant slowly. After supernatant was mixed very well, supernatants were centrifuged at 3900 rpm for 90 minutes at 8ºC. T213R/T214I CYP119 pellets from ammonium sulphate precipitation were dissolved with triethanolamine buffer (50 mM) at pH 7.3 and dialyzed against desalting buffer and 50 mM TEA buffer. 10 µL samples were taken for further purity analysis by SDS-PAGE.

T213R/T214I CYP119 protein concentrations were measured based on known extinction coefficient (ε_{415nm}=104mM^{-1} cm^{-1}). Protein isolation steps were illustrated in Figure 2.1.

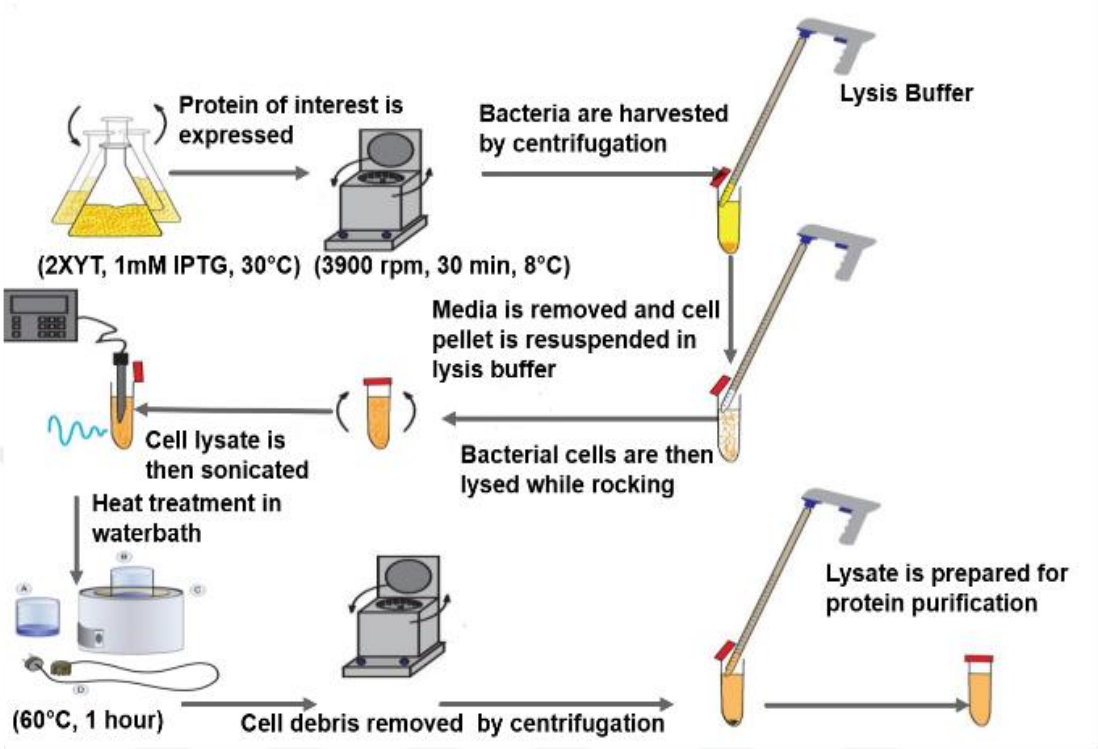

Figure 2.1 Protein isolation steps are demonstrated.

2.6 UV-Visible Spectra of WT CYP119 T213R/T214I CYP119

WT CYP119 and T213R/T214I CYP119 were analyzed under the UV-Visible spectra in 50 mM potassium phosphate at pH 7.4. Analysis was performed by 1600PC Scanning Spectrophotometer for WT and T213R/T214I CYP119.

2.7 Reactions of and WT CYP119 and T213R/T214I CYP119 with H_2O_2 and Cumene Hydroperoxide

The reactions of WT CYP119 and T213R/T214I CYP119 with H_2O_2 and cumene hydroperoxide reactions were analyzed by UV-Visible spectroscopy.and heme Soret absorbance was followed at 414 nm. Reaction mixtures contained 1.5 mM H_2O_2 or cumene hydroperoxide, T213R/T214I CYP119 and 1 mM EDTA, and 1.5 µM of enzyme (CYP119 or T213R/T214I CYP119) in 50 mM potassium phosphate at pH 7.4. Reaction volume was 700 µl. Blank was 50 mM potassium phosphate buffer at pH 7.4. Enzyme

was first monitored between 350 nm and 650 nm. After addition of peroxide, UV–Visible spectra were taken at 0, 2, 5, 10, 20, 30, min after the addition of peroxide.

2.8 Peroxidase Activity of T213R/T214I CYP119

2.8.1 Amplex® Red Reaction with T213R/T214I CYP119

Amplex® Red (Thermo Fisher Scientific) oxidation reaction was performed with T213R/T214I CYP119. Reactions mixture contains10 μM Amplex® Red, 1.5 mM H_2O_2, 1 mM EDTA and 1.5 μM CYP119 variants in 50 mM potassium phosphate at pH 7.4. The reactions were run at room temperature. Production of resorufin was analyzed by fluorescence monitoring. (570 nm excitation on, 585 nm emission) or absorbance at 570 nm. ($\mathcal{E}_{570nm}$ = 54 $mM^{-1} \cdot cm^{-1}$)

2.8.1.1 Kinetic Analysis of Amplex® Red Oxidation by T213R/T214I CYP119

Amplex® Red reaction was performed with WT CYP119 and T213R/T214I CYP119 and examined under the UV-Vis Spectroscopy. Reactions contained on 10 μM Amplex® Red, 1.5 mM H_2O_2 and 1.5 μM WT CYP119 and T213R/T214I CYP119 in 50 mM reaction buffer at pH 7.5. UV-Visible spectra were taken at 0, 2, 5, 10, 20, 30, 45, 60, 90, 120 minutes after the addition of H_2O_2. Amplex® Red reactions with CYP119s were analyzed under the different H_2O_2 concentrations (0.5 mM-2.5 mM) for determination of kinetic parameters. Initial rate was calculated by linear fitting. Lineweaver-Burk Plot was drawn by using initial rates for comparison. Kinetic parameters were determined by non-linear fitting with Michelis Menten equation. Michelis-Menten equation is shown in equation 2.

Equation 2: Y = Vmax*X/(Km+X) **(2)**

2.8.2 Guaiacol Oxidation Reaction with WT CYP119 and T213R/T214I CYP119

Guaiacol oxidation reaction was analyzed in the presence of WT CYP119 and T213R/T214I CYP119. Reaction mixtures contained 5 mM guaiacol, 1 mM H_2O_2 and 3 μM WT CYP119 and T213R/T214I CYP119 in a 50 mM reaction buffer at pH 7.4. UV-Reaction volume was 700 μl and quartz cuvette was used. Buffer, enzyme and guaiacol were put into the cuvette before measurement. After addition of H_2O_2, UV Visible spectra were taken from 350 to 650 nm at 1 min intervals for 20 min. The rate of tetraguaiacol formation is followed at 470 nm ($\mathcal{E}_{470nm}$ = 2.66 × 10^4 $M^{-1}cm^{-1}$)

2.8.3 ABTS Oxidation Reaction with T213R/T214I CYP119

The ABTS oxidation catalyzed by WT CYP119 and T213R/T214I CYP119 was examined at room temperature in 50 mM potassium phosphate buffer at pH 7.4. ABTS oxidation reaction was performed in quartz cuvette. Reaction volume was 700 μl containing 3 μM enzyme, 1 mM H_2O_2, 1 mM ABTS and 50 mM potassium phosphate buffer at pH 7.4. Firstly, 50 mM potassium phosphate buffer was measured as blank. Then, enzymes were put into the buffer and 1mM ABTS was added into the cuvette. Reactions were started with addition of 1 mM H_2O_2 added into the cuvette. The reactions were followed by 1 min interval from 950 nm to 350 nm for 45 minutes. The rate of the $ABTS^{+\cdot}$ cation radical formation by WT CYP119 and T213R/T214I CYP119 was also assessed by using the extinction coefficient of $ABTS^{+\bullet}$ at 734 nm ($\mathcal{E}_{734nm}$ = 1.5 × 104M^{-1} cm^{-1}).

2.8.4 Styrene Epoxidation Reaction

Styrene epoxidation was analyzed at room temperature in closed glass vials, the reaction was stopped after 10 min. The reaction mixture (100 μL) containing WT CYP119 or T213R/T214I CYP119 enzyme (12.5 μM), variable concentration of styrene (3-7 mM) (from a acetonitrile stock solution) and 7 mM *tert*-butyl hydroperoxide (TBHP) as oxidant in 50 mM potassium phosphate buffer (pH 7.4). The reaction was stopped by adding acetonitrile (900 μl). Reaction mixture was analyzed by HPLC on Thermo Scientific Ultimate 3000 coupled with UV detector fixed 220 nm. 25 cm Nucleodur C18 column (Macherey-Nagel) was used with 30% ddH_2O/ 70% acetonitrile as mobile phase. The retention times of styrene and styrene oxide were determined under this condition,

respectively 6.5 min and 4.27 min. Calibration curve was plotted by using (±)-styrene oxide 98+% and integration peak areas to calculate concentration of styrene oxide from reaction.

2.9 Substrate Binding Studies with T213R/T214I CYP119

2.9.1 Lauric Acid Binding Assay

Binding constants of T213R/T214I CYP119 and WT were determined at room temperature by difference spectroscopy. Enzyme solutions for WT CYP119 (1.5 μM) or T213R/ T214I (1.5 μM) were prepared in 50 mM potassium phosphate buffer at pH 7.4. Enzyme solutions were kept for 10 min at room temperature and divided into two glass cuvettes. Lauric acid in a dimethyl sulfoxide (DMSO) stock solution was titrated into the sample cuvettes containing WT CYP119 and T213R/T214I CYP119. Lauric acid (0.5 mM, 1 mM, 2 mM, 5 mM, 10 mM and 20 mM) was added into the cuvettes respectively. After addition of each solution, 5 minutes were waited, and UV spectra were taken between 350 nm and 650 nm for each concentration. Equal volume of dimethyl sulfoxide (DMSO) was added to control cuvettes containing WT CYP119 and T213R/T214I CYP119. The concentration of DMSO in the cuvette did not pass 1% of the underlying volume. The absorbance shift was monitored between 386 and 418 nm was followed. The shift was drawn against substrate concentration by nonlinear fitting. The shift from 386 to 418 nm was followed. The dissociation constant *(K_d)* was then determined by fitting plots of Δ386 – Δ418 against substrate concentration to the quadratic quadratic equation 3 [55]:

Equation 3 Formula of calculation of K_d and Amax value is illustrated in equation.

$$\Delta A = A_{\max}\left(\frac{K_d + [E] + [L] - \sqrt{(K_d + [E] + [L])^2 - 4[E][L]}}{2[E]}\right) \quad \textbf{(3)}$$

2.9.2 Progesterone Binding Assay

Binding constants of T213R/T214I CYP119 were analyzed at room temperature by difference spectroscopy, utilizing VWR® UV/1600PC Scanning Spectrophotometer.

Progesterone in a DMSO stock arrangement was titrated into the control cuvette containing 1.5 μM CYP119 in 50 mM phosphate buffer at pH 7.4. Progesterone (10, 20, 40, 60, 80, 100, 120, 140, 160 mM) were added into the cuvettes respectively. According to concentrations, same volume of DMSO was added into the control cuvette. Five minutes were waited after adding each substrate. UV spectra were taken two times between 350 nm and 650 nm. The shift was plotted against substrate concentration. The dissociation constant *(K_d)* was then determined by fitting plots of $\Delta 420 - \Delta 388$ against substrate concentration to the quadratic quadratic equation 3 described above.

2.10 Microtiter Plate Screening of T213R/T214I CYP119 reactivity under the methanol ethanol isopropanol and acetonitrile

Organic solvents effects on T213R/T214I CYP119 and WT CYP119 peroxidase activity were analyzed by using 96-well cell culture plate (VWR, 734-2781). Amplex® Red peroxidation assay was modulated by organic solvents. Each well has a total of 100μL reaction volume containing H_2O_2 (1 mM) Amplex® Red (10 μM), WT CYP119 (1.5 μM) or T213R/T214I CYP119 (1.5 μM) with different concentrations of organic solvent (0% v/v, 2.5% v/v, 5% v/v, 7.5% v/V, 10% v/v) in 50 mM potassium phosphate buffer at pH 7.4.

Blank used in the assay was 50 mM potassium phosphate buffer. Positive control was 1 μUnit HRP with H_2O_2 (1 mM), Amplex® Red in 50 mM potassium phosphate buffer at pH 7.4. All components were mixed before adding H_2O_2. Fluorescence emitted by resorufin was measured at 595 nm by using FLUOstar Omega (BMG LABTECH).

2.11 Peroxidation Activity of WT CYP119 and T213R/T214I CYP119 based on variable pH

Amplex® Red peroxidation reaction of WT CYP119 and T213R/T214I CYP119 were analyzed at various pH values. Reaction mixtures contained 1.5 μM enzyme (WT CYP119 or T213R/T214I CYP119), 10 μM Amplex® Red, 1.5 μM H_2O_2 in a 50 mM potassium phosphate buffer. Each potassium phosphate buffer was prepared at different pH values (5.8, 6.8, 7.4, and 8.0). The resorufin formation was observed at 570 nm during 45 min, with 2 min intervals.

2.12 Thermostability Measurements of WT CYP119 and T213R/T214I CYP119

Thermostability of WT CYP119 and T213R/T214I CYP119 were analyzed with increasing temperatures. Firstly, enzyme in 50 mM potassium phosphate buffer at pH 7.4 was incubated for 5 min at each temperature; 25, 40, 60, 70, 75, 80, 85, 90, and 95°C and 100°C respectively. UV-Visible spectra for enzyme solutions were monitored for each temperature between 350 nm and 650 nm . UV-Visible spectrum of the enzyme solution at room temperature was subtracted from the UV-Visible spectra of enzyme at higher temperatures, which was plotted as difference spectra. The change in Soret absorbance was examined according to literature [49].

2.13 Docking Studies of WT CYP119 and T213R/T214I CYP119 with Different Substrates

First, 1F4T.pdb file was taken from the RCSB PDB database. 1F4T is used crystal structure of WT CYP119. Before initialization of docking, clean pdb were prepared. All water molecules and cofactors were removed from PDB files with using cleanATOM protocol of the PyRosetta program.

PDB files must be prepared before starting the design process. That preparation includes removing all water molecules and cofactors from the PDB file. All non-Atom lines were removed from the original pdb file by using the below script.

```
from rosetta.toolbox import cleanATOM
cleanATOM("pdb_name" + ".pdb")
```

New pdb file was saved as pdb_name.clean.pdb.

After preparation of 1F4T.clean.pdb, HEM.pdb was prepared via UCSF Chimera. Hem files put into the molfile2params files.

"run molfile_to_params.py HEM.mol2 -n HEM"

HEM.params file was created by using the above string. This file is put into the residue_types file.

On the other hand, ligand smile string was taken from PubChem. Then, energy minimization of ligand was done for UCSF Chimera. 1F4T.pdb file and minimized ligand were opened and ligand grid lines was placed close to the active site of 1F4T. Then, pre-

docking of ligand was performed by AutoDock.vina. After docking, the lowest score was saved. Ligand was selected and saved as a pdb file.

Mutations on the structure of CYP119 was created by the Pyrosetta program. The Task Factory module of Pyrosetta is used for creation of mutations. Optimization of conformation of mutant residues was performed by the PackRotamersMover function based on the "REF2015" score function. Fast relax method was realized for energy minimization of WT CYP119 and T213R/T214I CYP119 structures. Fast relax method used the "REF2015" protocol as an energy function. After that, ligand docking was done by the DockMCMProtocol of the PyRosetta. 100 rounds of docking were performed. Docking protocol of CYP119 and T213R/T214I CYP119 were applied by using improvement and optimized protocol in our laboratory by Ekin Kestevur Doğru. Docking score of WT CYP119 and T213R/T214I CYP119 were estimated for different ligands. (Guaiacol, Amplex® Red, Progesterone, Testosterone, Indole, Indoxylacetate, Caffeine and SDS) by PyRosetta energy function. The lowest Rosetta Energy Unit (REU) scores were chosen for analysis of ligand–protein interactions. Ligand docking of protein images were obtained with the UCSF Chimera software.

CHAPTER 3

RESULTS AND DISCUSSION

T213R/T214I CYP119 was obtained by targeted directed evolution in our laboratory. This mutant was chosen from a high throughput screen following peroxidation activity of CYP119 mutants with the substrate Amplex® Red. The expression plasmid used in this thesis was isolated from a colony that showed increase peroxidation activity for Amplex® Red compared to WT CYP119. The plasmid was sent to sequence analysis. Sequence result showed that the improved mutant was T213R/T214I CYP119 [50].

3.1 Results of Expression and Isolation of T213R/T214I CYP119

E. coli BL21 (DE3) containing Pet11a expression vector coding for T213R/T214I CYP119 gene was grown overnight in LB Broth with 0.1 mg/mL ampicillin. The cells were inoculated from overnight culture into the 2xYT medium at pH 6.8. After OD reaches 0.7, protein expression is induced by 1mM IPTG. Expression of T213R/T214I CYP119 was followed by SDS PAGE analysis as seen in Figure 3.1. The molecular weight of T213R/T214I CYP119 is 43 kDa so the protein was observed between 35 kDa and 45 kDa. In Figure 3.1 the first two lanes show before IPTG induction (1) and after IPTG induction (2). Overexpression of T213R/T214I CYP119 is observed in lane 2. Isolation of T213R/T214I CYP119 was described in the 2.3 SDS-PAGE analysis section. Isolation of T213R/T214I CYP119 was followed by 15% SDS-PAGE Analysis (Figure 3.1). The steps of isolation can be described briefly as lysis (3), sonication (4), heat treatment (5), centrifugation (6, 7), %30 ammonium sulphate precipitation (8, 9), , %60 ammonium sulphate precipitation (10), and dialysis. Since CYP119 is a thermophilic enzyme and it is stable at high temperatures. To remove nonstable proteins, heat treatment is applied to cell lysate at 60ºC for one hour during purification of T213R/T214I CYP119.

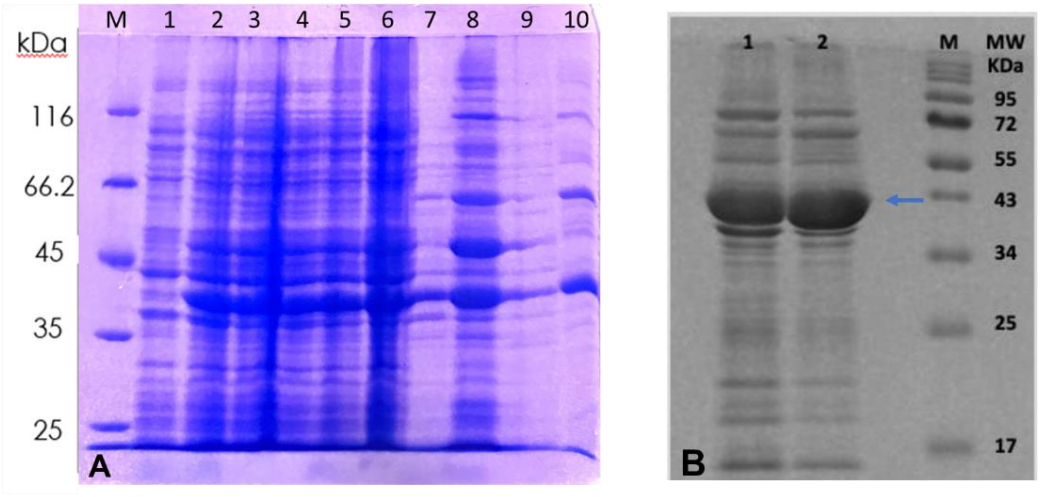

Figure 3.1 SDS-PAGE analysis of T213R/T214I CYP119 expression and isolation (A). M: protein molecular weight marker. Lane 1: before IPTG addition, lane 2: after IPTG addition, lane 3: lysis, lane 4: sonication, lane 5: heat treatment, lane 6: pellet, lane 7: supernatant, lane 8: 30% ammonium sulphate precipitation (supernatant), lane 9: 60% ammonium sulphate precipitation (supernatant), lane 10: pure enzyme after dialysis . SDS-PAGE analysis of T213R/T214I and WT CYP119 after isolation (B). M: protein molecular weight marker (NEB #P7719S). Lane 1: T213R/T214I CYP119 after purification. Lane 2: WT CYP119 (43 kDa) after purification.

During heat treatment, unstable *E.coli* proteins were denaturated. Then, cell lysate was centrifuged, most of the unwanted proteins were removed in this step. 30% amount of ammonium sulphate was added into the supernatant of T213R/T214I CYP119. After centrifugation, precipitated protein was removed. Then, 60% amount of ammonium sulphate was added into the supernatant. After centrifugation, obtained pellet was dissolved with 50 mM triethanolamine at pH 7.3. Obtained T213R/T214I CYP119 was dialyzed against to same buffer. Enzyme was collected from the column and concentrated by protein concentrators with 10 K molecular weight cut-off. After isolation, WT CYP119 and T213R/T214I CYP119 had similar purities as seen in SDS PAGE analysis (Figure 3.1B).

3.2 UV-Visible Spectral Analysis of WT CYP119 and T213R/T214I CYP119

UV-Visible spectra of T213R/T214I CYP119 and WT CYP119 were investigated. WT CYP119 (1.5 μM) and T213R/T214I CYP119 (1.5 μM) in 50 mM

potassium phosphate at pH 7.4 were analyzed in UV-Visible spectra. The optical spectra of WT CYP119 and T213R/T214I CYP119 are shown in Figure 3.2. WT CYP119 shows maximum Soret absorbance at 414 nm and split α/β bands at 531 and 564 nm similar to previously reported spectra [17]. The T213R/T214I mutation did not cause a significant Soret shift with a Soret maximum at 415 nm; but broadening of the Soret absorbance and α/β bands were observed. (Figure 3.2).

Isolated and purified enzyme were analyzed in UV-Visible spectra. Heme incorporation of T213R/T214I CYP119 was examined from 415 nm (Soret) and 280 nm ratio. This ratio was 0.45 and 0.65 for T213R/T214I CYP119 and WT CYP119 respectively. They show appropriate levels of heme incorporation for both proteins.

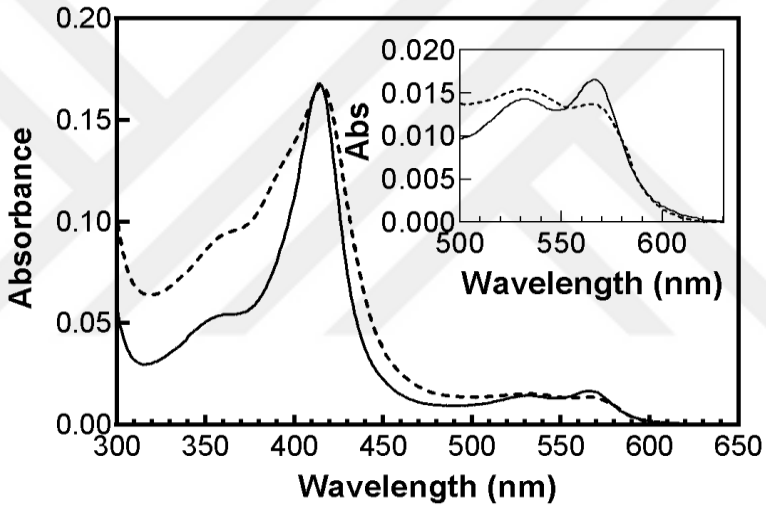

Figure 3.2 UV–Visible Spectra of T213R/T214I CYP119 and WT CYP119 were demonstrated. (solid: WT CYP119; dash: T213R/T214I CYP119). Inset: The alterations observed in the alpha–beta region)

Distal water ligand is more firmly bound to iron atom in CYP119 in contrast to other P450s, so CYP119 is at low spin, and shifting CYP119 heme iron from low spin to high spin is difficult[2]. Substitution of Thr214 and Thr213 with large amino acids significantly alters spin state of heme iron which may result in broadening of Soret peak of T213R/T214I CYP119.

3.3 Peroxidase Activity of Analysis of WT CYP119 and T213R/T214I CYP119

3.3.1 Peroxidation of Amplex® Red catalyzed by WT CYP119 and T213R/T214I CYP119

The Amplex® Red peroxidation reaction was catalyzed by WT CYP119 and T213R/T214I CYP119 in the presence of H_2O_2. Peroxidation reaction was monitored by UV- Visible spectra [48]. Reaction mixture include Amplex® Red (10 μM), H_2O_2 (1.5 mM), enzyme (1.5 μM) in 50 mM potassium phosphate buffer at pH 7.4. Amplex® Red is a colorless substrate. During the reaction, Amplex® Red is oxidized to resorufin which is fluorescent and at 570 nm (Figure 3.4). Amount of resorufin product formation is measured by using its extinction coefficient at 570 nm [56]. While WT CYP119 catalyzed oxidation of 7% of Amplex® Red, T213R/T214I CYP119 catalyzed oxidation of 60% of Amplex® Red according to the final amount of produced resorufin. Hence, the peroxidation activity of T213R/T214I CYP119 has an 8-fold higher yield of Amplex® Red peroxidation compared to WT CYP119 .

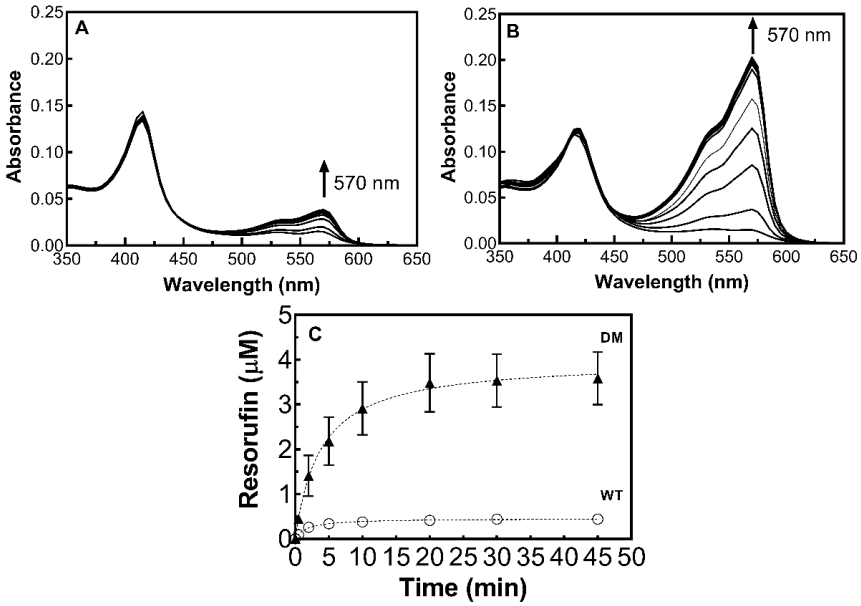

Figure 3.3 Amplex® Red oxidation during the reaction catalyzed by WT CYP119 (A) and T213R/T214I CYP119 (B); in the presence of H_2O_2 were monitored by UV-Visible spectra. UV-Visible spectra were taken at 0, 2, 5, 10, 20, 30, and 45 min after the addition of H_2O_2. The reactions contained10 μM Amplex® Red, 1.5 mM H_2O_2, and 1.5 μM enzyme, and 1 mM EDTA in 50 mM potassium phosphate buffer at pH 7.4. Resorufin formation was followed at 570 nm for WT CYP119 (empty circle) and T213R/T214I CYP119 (DM, filled triangle) (C) in the same reaction.

3.3.1.1 Kinetic Analysis of Amplex® Red Peroxidation of T213R/T214I CYP119 and comparison of WT CYP119

In this study, kinetic parameters for Amplex® Red oxidized by these proteins were examined (Figure 3.6). Amplex® Red peroxidation was followed with variable (0.5- 2.5 mM) H_2O_2 concentrations. The initial rate of resorufin formation was obtained for each reaction by linear fitting. Lineweaver Burk Plot was drawn by using initial rate of each concentrations. Kinetic parameters were determined by non-linear fitting. The k_{cat} was determined to be $2.1 \pm 0.3 \times 10^{-3}$ s^{-1} for WT and $1.1 \pm 0.13 \times 10^{-2}$ s^{-1} for the T213R/T214I CYP119. There was a 5-fold increase in the k_{cat} observed for T213R/T214I CYP119 compared to WT CYP119. While the K_m of WT CYP119 for H_2O_2 was determined to be 0.82 ± 0.46 mM, K_m of T213/T214I CYP119 for H_2O_2 was determined as 1.32 ± 0.3 mM. When K_m values for WT CYP119 and T213R/T214I CYP119 were compared, mutations on Thr213 and Thr214 residues caused to small changes in K_m values for CYP119.

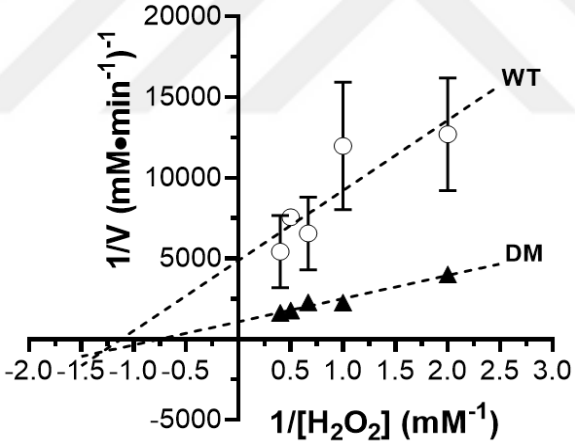

Figure 3.4 Investigations of the kinetic parameters of Amplex® Red oxidation by WT CYP119 (empty circle) and T213R/T214I CYP119 (DM, filled triangle). in the presence of H_2O_2. Reactions involved 10 µM Amplex® Red, 1.5 µM T213R/T214I or WT CYP119, and variable concentrations (0.5– 2.5 mM) of H_2O_2 in 50 mM potassium phosphate buffer, pH 7.4

T213R/T214I CYP119 shows higher Amplex® Red peroxidation activity than WT CYP119. Comparison of Amplex® Red peroxidation activity of T213R/T214I CYP119 and WT CYP119 shows that two mutations in active site may cause increased activity towards H_2O_2. Because determination of kinetic parameters of the peroxidation reaction

was not analyzed under saturating concentrations of Amplex® Red, the alterations in k_{cat} can also be because of changes in the affinity for Amplex® Red.

3.3.2 Oxidation Reaction with Guaiacol by CYP119 and T213R/T213I CYP119

As mentioned above, T213R/T214I CYP119 was selected due to demonstration of increased peroxidase activity for Amplex® Red. We wanted to study if this increase in peroxidation can also be observed for other substrates. T213R/T214I CYP119 and WT CYP119 were investigated in terms of catalyzation of guaiacol oxidation reaction in the presence of H_2O_2. Reaction was initiated with WT CYP119 (3μM) or T213R/T214I CYP119 (3μM), guaiacol (5 mM,) H_2O_2 (1mM) in 50 mM potassium phosphate buffer at pH 7.4 and 25°C. The reactions were followed by UV–Visible spectra Figure 3.5. During the reaction, an increase at 415 and 470 nm can be observed (Figure 3.5). These bands can be attributed to tetraguaicol formation [54] .When UV-Visible Spectra of guaiacol oxidation was examined in the presence of WT CYP119, there was no increase in absorbance at 470 nm (Figure 3.7B). WT CYP119 did not catalyze tetraguaiacol formation. The only changes observed in the WT CYP119 reaction is the decrease of heme Soret at 414 nm. Because H_2O_2 causes bleach of heme. Although WT CYP119 does not perform the oxidation reaction for guaiacol substrate, T213R/T214I CYP119 showed oxidation activity. Mutation on Thr213 and Thr214 residues changed active site of the enzyme for the guaiacol substrate.

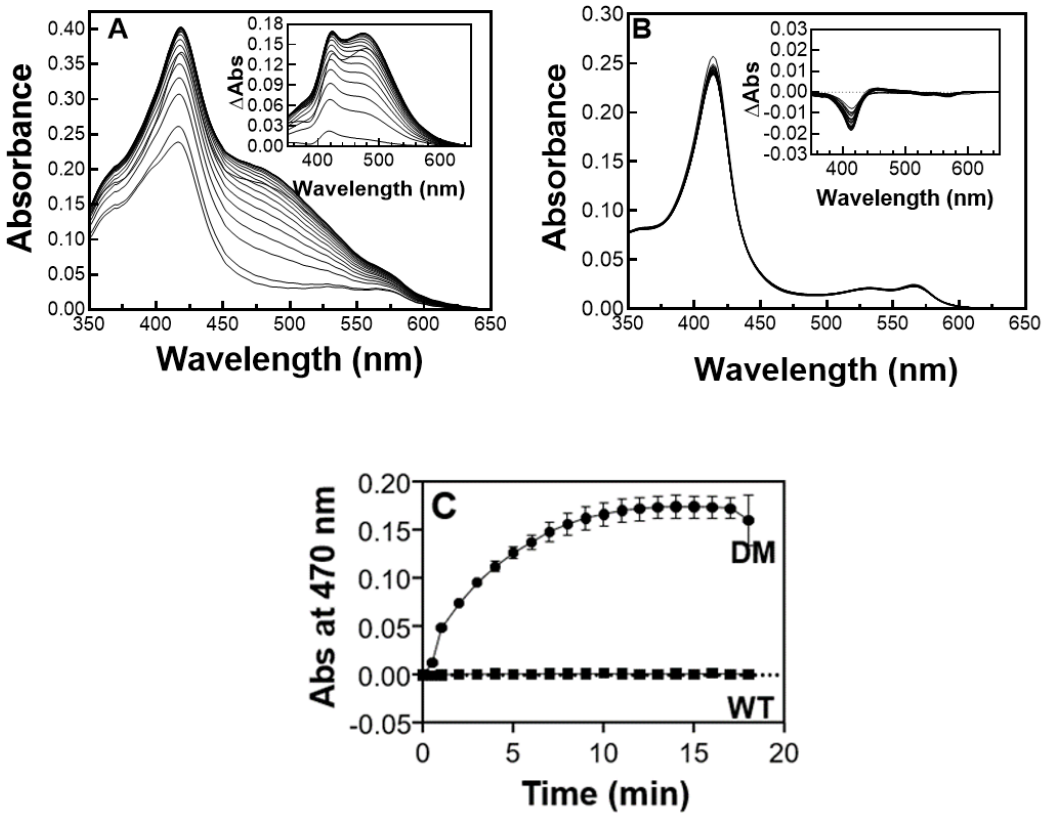

Figure 3.5 Oxidation of guaiacol catalyzed by T213R/T214I CYP119 (A) and WT CYP119 (B) in the presence of H_2O_2. H_2O_2 (1 mM) was added to enzymes (3 μM) T213R/T214I CYP119 and WT CYP119 and guaiacol (5 mM) mixture in 50 mM phosphate buffer at pH 7.4 and 25°C. The spectra were taken at 1 min intervals for 20 min. The product for the reaction, tetraguaiacol shows absorbance at 470 nm during the reaction. Time course of guaiacol oxidation in the presence of WT CYP119 and T213R/T214I CYP119 (C).

3.3.3 Oxidation Reaction of ABTS by WT CYP119 and T213R/T214I CYP119

One electron oxidation of 2,2'-azino-bis(3-ethylbenzothiazoline-6-sulfonic acid (ABTS) by H_2O_2 in the presence of WT CYP119 and T213R/T214I CYP119 was investigated. The reaction mixtures contain ABTS (1mM), H_2O_2 (1 mM), WT CYP119 (1 μM) and T213R/T214I (1 μM) in potassium phosphate buffer at pH 7.4. Reaction was monitored at 25 °C by UV-Visible Spectra. ABTS radical cation formation can be observed by a broad band at 734 nm.

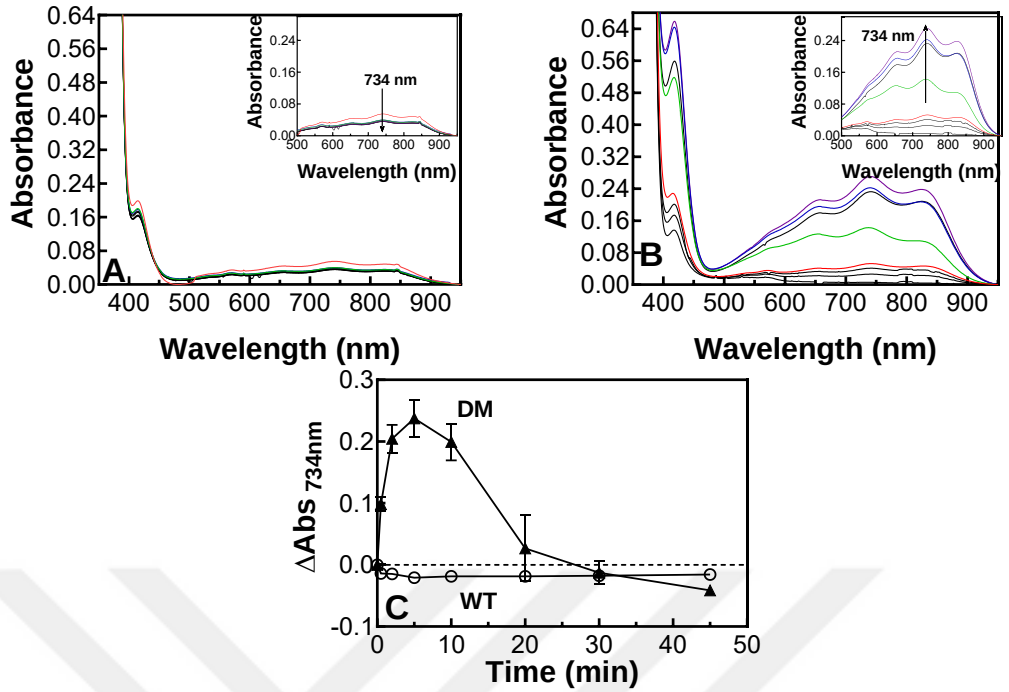

Figure 3.6 Oxidation reaction of ABTS catalyzed by WT CYP119 and T213R/T214I CYP119 in the presence of H_2O_2. Reaction contained WT CYP119 (1µM) in A and T213R/T214I CYP119 (1µM) in B, H_2O_2 (1mM), ABTS (1mM), in 50 mM potassium phosphate buffer at 25ºC and pH 7.4. The spectra were taken between 350 and 950 nm at 0-(red), 0-(+H_2O_2,green), 2(blue)-, 5(purple) -, 10-, 20-, 30- and 45-min. Production of $ABTS^{\cdot+}$ was monitored at 734 nm appears during the reaction (C). Time course of ABTS oxidation in the presence of WT CYP119 and T213R/T214I CYP119 were observed.

We found that T213R/T214I CYP119 can perform catalytic turnover of the peroxidase substrate, ABTS to generate $ABTS^{\cdot+}$ cation radical (Figure 3.8). Maximum absorbance at 734 nm were recorded after 5 min with T213RT214I CYP119. Observed peak in 734 nm decreases after 45 min due to oxidation of the $ABTS^{\cdot+}$ radical by another electron and production of azodication ($ABTS^{2+}$). This reaction is shown in the equation 4 below:

Equation 4: $ABTS \rightarrow ABTS^{\cdot+} + e^{-} \rightarrow ABTS^{2+} + e^{-}$ **(4)**

3.4 Styrene Epoxidation Reaction Catalyzed by WT CYP119 and T213R/T214I CYP119

To investigate the epoxidation activity for WT CYP119 and T213R/T214I CYP119, styrene was chosen as a substrate. The styrene epoxidation reactions performed with tert-Butyl hydroperoxide (TBHP) as an oxidant was applied at 25 °C and pH 7.4. Pure styrene and styrene oxide were used for creating of calibration curves in HPLC analysis. The rate of styrene epoxidation reaction was investigated by HPLC analysis with the assistance of these calibration curves. Kinetic parameters were determined by nonlinear fitting analysis with different concentrations of the substrate styrene as described in Figure 3.9. The k_{cat} was obtained $5 \pm 0.1 \times 10^{-2}$ s^{-1} for WT CYP119 and $11.7 \pm 0.5 \times 10^{-2}$ s^{-1} for T213R/T214I CYP119. The K_m value of WT CYP119 and T213R/T214I CYP119 were obtained as 14.8 ± 3.2 mm and 14.0 ± 8.3 mM, respectively. Consequently, T213R/T214I CYP119 demonstrated elevated k_{cat} of styrene epoxidation without change substrate affinity

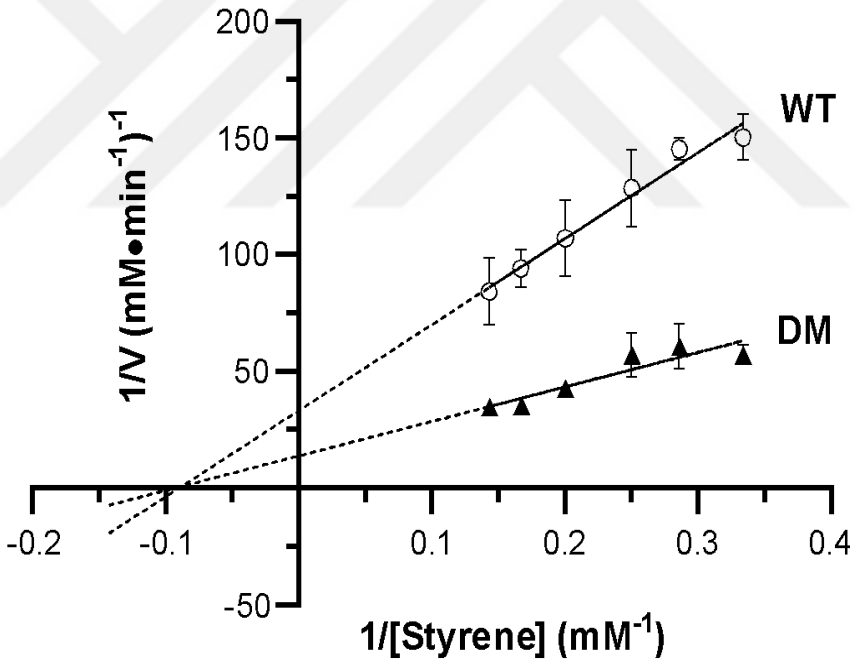

Figure 3.7 Determination of the kinetic parameters of styrene epoxidation by variable concentrations of styrene (3–7 mM) in the presence of WT CYP119 (empty circle) and T213R/T214I CYP119 (DM, filled triangle). Reactions contained variable concentration styrene (3–7 mM), 7 mM TBHP, and 12.5 μM enzyme in 50 mM potassium phosphate buffer at pH 7.4 and 25 °C for 10 min.

Although T213R/T214I CYP119 was selected for increased Amplex® Red peroxidation by the assay, activity of enzymes for other substrates were also investigated.

One of these substrates is styrene. Therefore, styrene epoxidation was investigated for T213R/T214 CYP119. TBHP was chosen as oxidant because according to previous studies, TBHP is a good oxidant for styrene epoxidation in contrast to other oxidants like H_2O_2 and cumene hydroperoxide so that in this reaction [48].

There was a two-fold increase in the catalytic activity of styrene epoxidation by the T213R/T214I CYP119. The k_{cat} obtained were $5 \pm 0.1 \times 10{-}^{2}s^{-1}$ for WT CYP119. and $11.7 \pm 0.5 \times 10^{-2}$ s^{-1} for T213R/T214 mutant. K_m values were obtained 14.8 ± 3.2 mM for WT CYP119 and 14.0 ± 8.3 mM for T213R/T214I CYP119. Though, k_{cat} of T231R/T214I increased in styrene epoxidation, K_m values of T213R/T214I CYP119 (14 mM) and WT CYP119 (14.8 mM) were similar. Therefore, mutation on T213R/T214I CYP119 did not change affinity for styrene significantly.

3.5 Reactions of WT CYP119 and T213R/T214I CYP119 with H_2O_2 and Cumene Hyroperoxide

H_2O_2 is an important oxidant that is used in peroxygenation reactions. Based on research, most P450s do not utilize H_2O_2 efficiently [57]. T213R/T214I CYP119 was showed for peroxidation activity in the presence of H_2O_2. In this study we want to analyze H_2O_2 effect on the enzyme without any substrates. In Figure 3.8, WT CYP119 (1.5 μM) or T213R/T214I CYP119 (1.5 μM) react with 1.5 mM H_2O_2 in potassium phosphate buffer at pH 7.4; changes in absorbance of the heme Soret was observed in the UV-Visible spectra during the reaction. Reaction of WT CYP119 with H_2O_2 causes a decrease in the peak at 414 nm in Figure 3.8A. The reaction was followed for 45 minutes at room temperature. Absorbance at 414 nm decreased by 15% during the reaction. The observed rate constant of WT CYP119 for the decrease in Soret absorbance was $1.8 \pm 0.6 \times 10^{-3}$ s^{-1}. The reaction of T213R/T214I CYP119 with H_2O_2 was also monitored by UV–Visible spectra. The reaction of T213R/T214I CYP119 with H_2O_2 did not result in a significant reduction in the maximum Soret absorbance. However, a narrowing of Soret band was observed in Figure 3.8B. A decrease in 390 nm was observed as seen in Figure 3.8B inset. While heme Soret at 414 nm of WT CYP119 significantly decreases, heme Soret of T213R/T214I CYP119 at 414 nm was not altered significantly during the reaction.

The reaction of T213R/T214I CYP119 with H_2O_2 was also investigated to understand how the mutation affects peroxides reactivity without other substrates. The heme cofactor of T213R/T214I CYP119 displayed high stability towards degradation by

H_2O_2 because no significant negative change in Soret absorbance at the end of the reaction (Figure 3.8). Difference spectra was analyzed to observe change on the heme iron . In the Figure 3.8 B inset, the shift of Soret of T213R/T214I CYP119 was observed. This shift in Soret absorbance can result into changes in the spin state of the heme iron to high spin. Mutations on Thr213 and Thr214 residues causes heme bleached slowly in the presence of H_2O_2[2]. This information is consistent with our observation that mutations on Thr213 and Thr214 residues result in increased Amplex® Red peroxidation activity. T213R/T214I CYP119 may be altered substrate affinity and reactivity of CYP119 towards peroxides.

Cumene hydroperoxide is an organic peroxide. The reaction between WT CYP119 and T213R/T214I CYP119 were investigated. WT CYP119 (1.5 μM) and T213R/T214I CYP119 (1.5 μM) reacted with cumene hyroperoxide (1.5 mM) and changes in heme Soret absorbance was observed by UV-Visible spectroscopy during the reaction. Reaction of WT CYP119 with cumene hydroperoxide caused a rapid decrease in absorbance at 414 nm (Figure 3.9A). The reaction of WT CYP119 and cumene hydroperoxide was followed for 45 minutes at room temperature. Absorbance at 414 nm decreased by 37%. However, an increase was observed in absorbance at lower wavelengths for 45 minutes due to aggregation of apoenzyme (Figure 3.9A).The observed rate constant of WT CYP119 for the decrease in Soret absorbance was $1.9 \times 10^{-4}\ s^{-1}$. The reaction of T213R/T214I CYP119 with cumene hydroperoxide was also monitored by UV–Visible Spectra. Absorbance of T213R/T214I CYP119 at 414 nm decreases by 36%. The observed rate constant of T213R/T214I CYP119 during the reaction was 1.3×10^{-4} s^{-4} as seen in Figure 3.9B. While, heme of WT CYP119 degraded with cumene hydroperoxide rapidly, heme of T213R/T214I CYP119 degraded more slowly. T213R/T214I CYP119 is more stable towards oxidation by cumene hydroperoxide compared to WT CYP119.

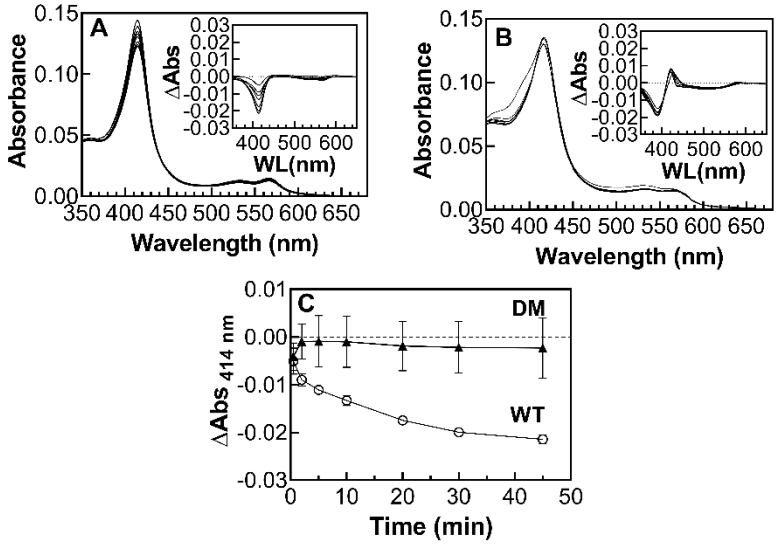

Figure 3.8 Effects of H_2O_2 reaction with WT (A) and T213R/T214I CYP119 (DM) (B).were displayed in UV-Visible spectra UV Visible spectra were monitored at 0, 2, 5, 10, 20, 30, and 45 min. Inset demonstrates difference spectra. Reaction involved 1.5 mM H_2O_2 , and 1.5 μM enzyme, 1 mM EDTA in 50 mM potassium phosphate buffer at pH 7.4. (C) Decrease in 414 nm of WT (empty circle) and DM (filled triangle).

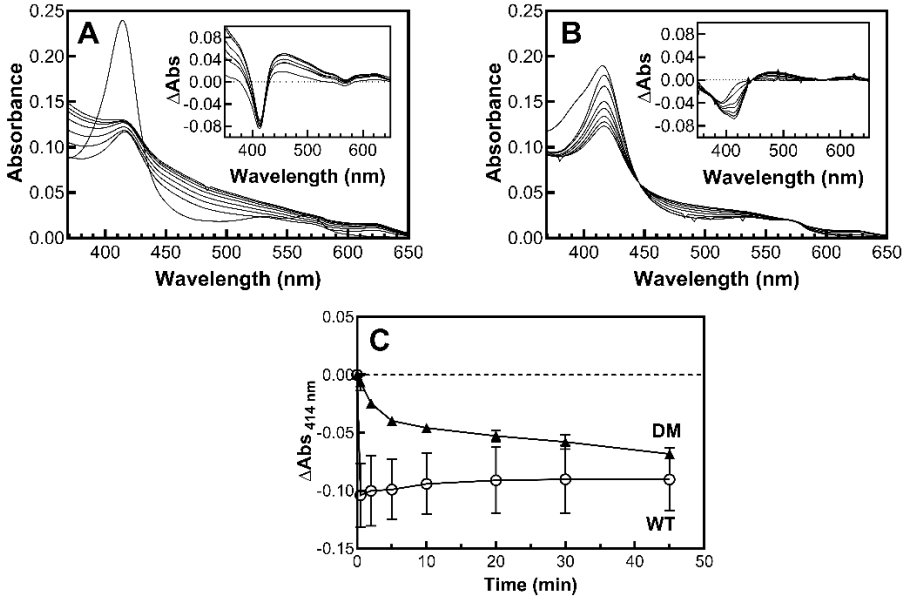

Figure 3.9 Reaction of cumene hydroperoxide reaction with WT CYP119(A) and T213R/T214I CYP119 (B).were observed by UV-Visible Spectra. UV-Visible Spectra. Spectra were taken at 0, 2, 5, 10, 20, 30, and 45 min. Inset demonstrates difference spectra. Reactions involved 1.5 mM H_2O_2 , and 1.5 μM enzyme, in 50 mM potassium phosphate buffer at pH 7.4. (C) Decrease in 414 nm for WT (empty circle) and DM (filled triangle)

3.6 Substrate Binding to WT CYP119 and T213R/T214I CYP119

Thr213 and Thr214 are located on the active site of the enzyme so mutation of these residues were expected to change substrate binding for CYP119. Therefore, the effects of these mutations on substrate binding were investigated.

3.6.1 Lauric Acid Binding of WT CYP119 and T213R/T214I CYP119

In this study, comparison of lauric acid binding to WT CYP119 and T213R/T214I CYP119 were analyzed. Dissociation constants (K_d) were obtained from alteration of magnitude of spin state of the CYP119 heme iron. Magnitude of spin state change is related to magnitude of the Soret absorbance shift (Figure 3.10). T213R/T214I CYP119 variant demonstrates larger Soret shift in UV-Visible Spectra analysis when compared to WT CYP119. Difference spectra were analyzed depend on rising lauric concentrations. Difference spectra were obtained by subtraction between 386 nm and 418 nm versus concentrations of lauric acid were drawn by nonlinear fitting (Figure 3.10A Figure 3.10B). Furthermore, T213R/T214I CYP119 variant illustrated four-fold lower affinity for lauric acid in contrast to WT CYP119. Because while K_d value of T213R/T214I was obtained to be 59.1 ± 30.2 μM, the K_d value of WT CYP119 was obtained as 16.8 ± 4.5 μM. Therefore, a four-fold decrease in the affinity for lauric acid is observed due to T213R/T214 mutation.

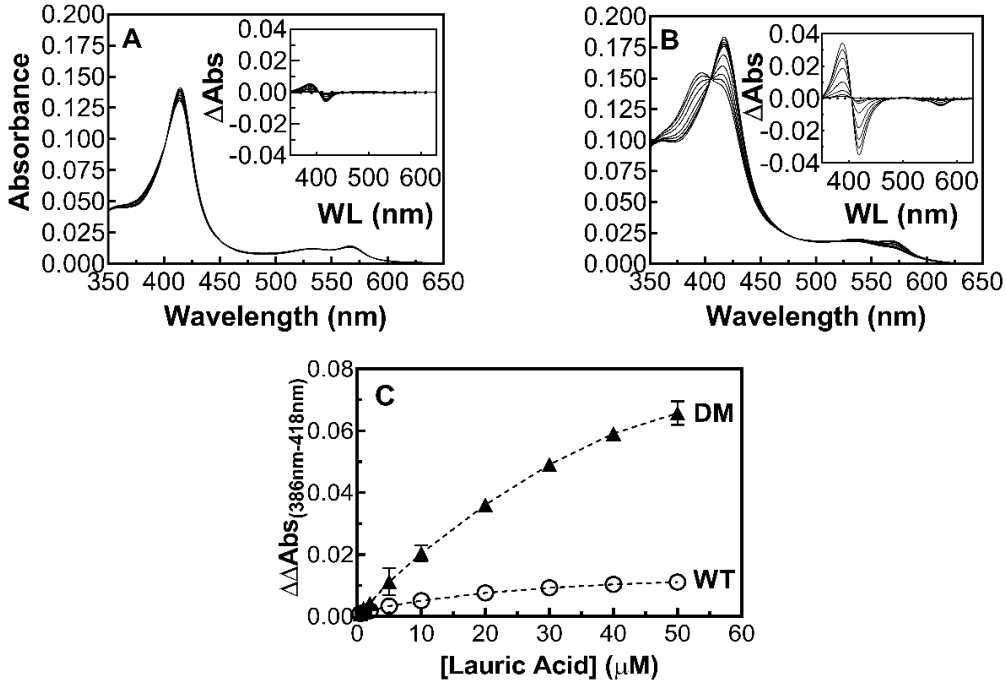

Figure 3.10 Changes in UV–Visible spectra of WT (A) and T213R/T214I CYP119 (B) with increasing concentrations of lauric acid.UV–Visible spectra of 1.5 μM WT CYP119 or T213R/T214I CYP119 were taken with variable concentrations of lauric acid (0.5 – 50 μM). Inset: difference spectra with rising lauric acid concentrations. The absorbance shifts are seen in 386 nm and 418 nm for lauric acid binding assay of WT CYP119 (empty circle) and T213R/T214I CYP119 (DM, filled triangle) (C). The absorbance subtraction between 386 nm and 418 nm versus concentrations of lauric acid were fit to quadratic equation to obtain K_d values nonlinear fitting.

3.6.2 Progesterone Binding to WT CYP119 and T213R/T214I CYP119

In this study, progesterone binding study was investigated for WT CYP119 and T213R/T214I CYP119. In the Figure 3.11, progesterone binding to WT CYP119 and T213R/T214I CYP119 were analyzed by UV Visible Spectra (Figure 3.11A and Figure 3.11B). The insets show difference spectra with different concentrations of progesterone the absorbance shifts are observed in 420nm and 388 nm for progesterone binding assay of WT CYP119 and T213R/T214I CYP119. The absorbance subtraction between 420 nm and 388 nm versus concentrations of progesterone were drawn by nonlinear fitting.

Difference spectra demonstrate that changes in the spin state of heme iron were observed with changes of Soret shift for WT CYP119 and T213R/T214I CYP119ö,. The Soret absorbance shifted from high spin to low spin in Figure 3A inset and 3B inset. The

K_d values for both of enzymes were obtained from analysis of the shift in Soret absorbance.

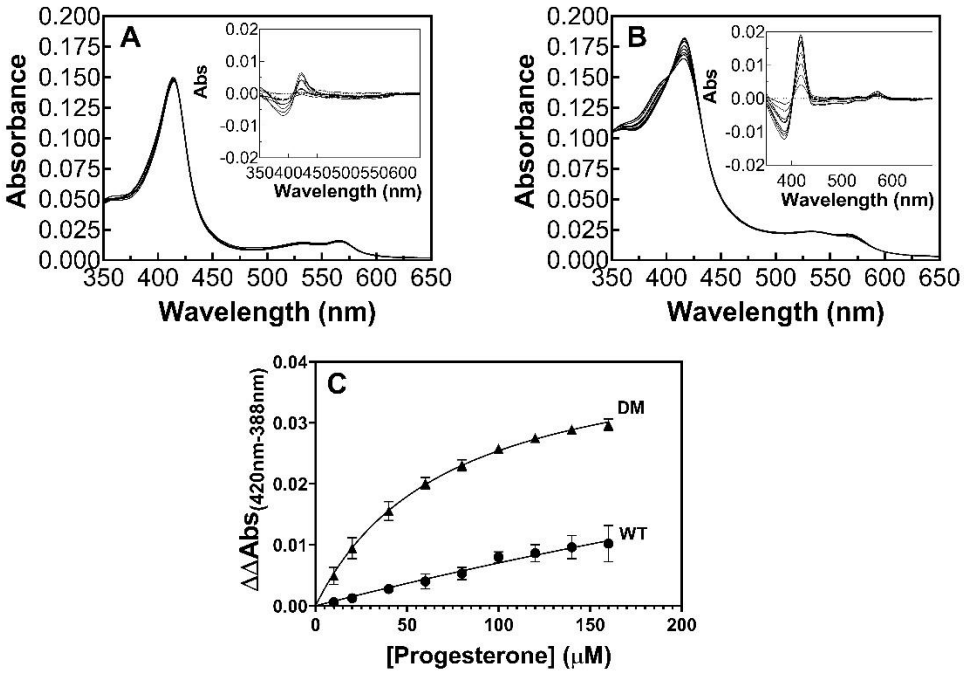

Figure 3.11 UV–Visible Spectra and difference spectra of WT (A) and T213R/T214I CYP119 (B) were demonstrated for progesterone binding study. UV–Visible spectra of 1.5 μM WT CYP119 or T213R/T214I CYP119 were taken with variable concentrations of progesterone (0.01–160 μM). The insets illustrate difference spectra with rising progesterone concentrations. (C) the absorbance shifts are observed in 420nm and 388 nm for progesterone binding assay of WT CYP119 (filled circle) and T213R/T214I CYP119 (DM, filled triangle). The absorbance subtraction between 420 nm and 388 nm versus concentrations of progesterone were drawn by nonlinear fitting

The K_d value of WT CYP119 is very high 755.3±428.6 μM. WT CYP119 has very low affinity for progesterone. In contrast, T213R/T214I CYP119 was higher affinity for progesterone. The K_d values for progesterone binding to T213R/T214I CYP119 was 71.2±17.2 μM. T213R/T214I CYP119 shows 11-fold higher affinity to progesterone compared to WT CYP119. For the first time, we report that an increase in progesterone affinity for T213R/T214I CYP119 for hydroxylation of progesterone. Mutations on Thr213 and Thr214 residues change the active site of CYP119. T213R/T214I mutation of CYP119 resulted in that active site becoming more suitable for progesterone binding.

3.7 Analysis organic of the effects on organic solvent on WT CYP119 and T213R/T214I CYP119

In this study, effects of methanol, isopropanol and acetonitrile were investigated on peroxidation activity of WT CYP119 and T213R/T214I CYP119. Organic solvents were applied to WT CYP119 and T213R/T214I CYP119 at 2.5% v/v, 5% v/v and 7.5% v/v concentrations. Inhibitory effect of organic solvents on WT CYP119 and T213R/T214I CYP119 were examined. Thermophilic enzymes shows organic solvent stability compared to mesophilic enzymes. As CYP119 is a thermophilic enzyme, effects of organic solvent on peroxidation activity of WT CYP119 and T213R/T214I CYP119 were investigated.

The effects of three commonly used organic solvents, methanol, acetonitrile and isopropanol on peroxidation activity of WT CYP119 and T213R/T214I CYP119 were examined. Peroxidation activity of WT CYP119 and T213R/T214I CYP119 was weakly inhibited as 10% at 2.5% v/v methanol. Approximately 23% inhibition of peroxidation activity of T213R/T214I CYP119 was observed at 5% v/v methanol and 7.5% v/v methanol.

Approximately 12% inhibition of peroxidation activity of WT CYP119 was observed at 5% v/v methanol. When the %7.5 v/v methanol was applied to WT CYP119, peroxidation activity was inhibited as 35%. (Figure 3.12A). Significant decreases in peroxidation activity of WT CYP119 were observed in the presence methanol (7.5 % v/v) compared to decrease in peroxidation activity of T213R/T214I CYP119.

Peroxidation activity was investigated in the presence of acetonitrile. Approximately 10% inhibition of peroxidation activity was observed in the presence of 2.5% v/v acetonitrile. 21% inhibition of peroxidation activity of T213R/T214I CYP119 was observed in the presence of 5% v/v acetonitrile while peroxidation activity of WT CYP119 was decreases as 24 % in the presence of 5 % v/v acetonitrile. When the concentration of acetonitrile reaches 7.5 v/v in the peroxidation reaction, 26 % inhibition of peroxidation activity of T213R/T214I CYP119 and 32% inhibition of WT CYP119 were observed. T213R/T214I CYP119 is more stable than WT CYP119 in the presence acetonitrile.

Isopropanol effect on peroxidation activity was investigated for T213R/T214I CYP119 and WT CYP119. %41 inhibition of peroxidation activity of T213R/T214I CYP119 and %13 inhibition of peroxidation activity of WT CYP119 were observed in the presence of 2.5 v/v isopropanol. Isopropanol inhibited peroxidation activity at lower concentrations for T213R/T214I CYP119 compared to WT CYP119. Approximately %50 inhibition of peroxidation activity of T213R/T214I CYP119 was observed at 7.5 v/v

isopropanol. Unlikely ,when the concentration reaches 5% v/v isopropanol, 36% inhibition of peroxidation activity of WT CYP119 was observed. 50% inhibition of peroxidation activity was observed the presence of 7.5 v/v isopropanol. The results demonstrate that T213R/T214I CYP119 shows more stability compare to WT CYP119 in the presence of high concentration of organic solvents. (Figure 3.12).

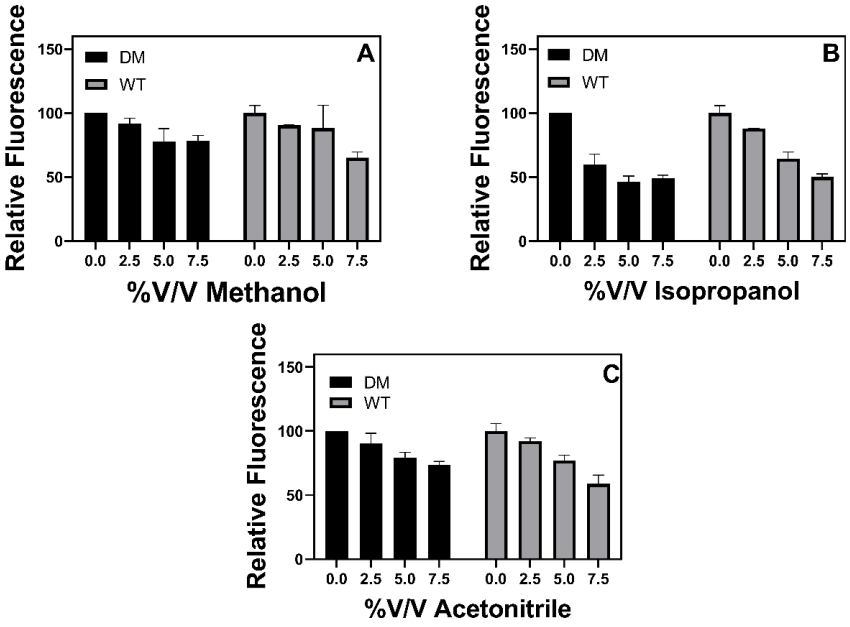

Figure 3.12 Screening of organic solvent effects on peroxidation activity of WT CYP119 (WT; gray) and T213R/T214I CYP119 (DM; black) were analyzed. Reactions contained variable concentrations of (2.5 ,5 ,7.5) % v/v methanol (A), isopropanol (B) and acetonitrile (C), 1.5 µM WT CYP119 and T213R/T214I CYP119, 1.5 mM H_2O_2 and 10 µM Amplex® Red in 50 mM buffer at pH 7.4. Positive control (PC; reaction without organic solvent).

Amplex® Red is a colorless substrate. Amplex® Red peroxidation reaction by peroxidase produce the fluorescent compound resorufin which has excitation maximum at 571 nm and emission maximum at 585 nm. Fluorescence activity of WT CYP119 and T213R/T214I CYP119 were analyzed in the Amplex® Red peroxidation reaction. Results show that mutant show higher peroxidation activity although organic solvent inhibits the peroxidation activity of the T213R/T214I CYP119 (Figure 3.13).

Generally, CYPs were incubated as purely aqueous incubation conditions. When an organic solvent desired to be used, methanol becomes more suitable than other organic solvents. These results are obtained by our observation that WT CYP119 and

T213R/T214I CYP119 were not inhibited more than 10% by 2.5 % v/v methanol. Likewise, acetonitrile demonstrates modest inhibitory effects.

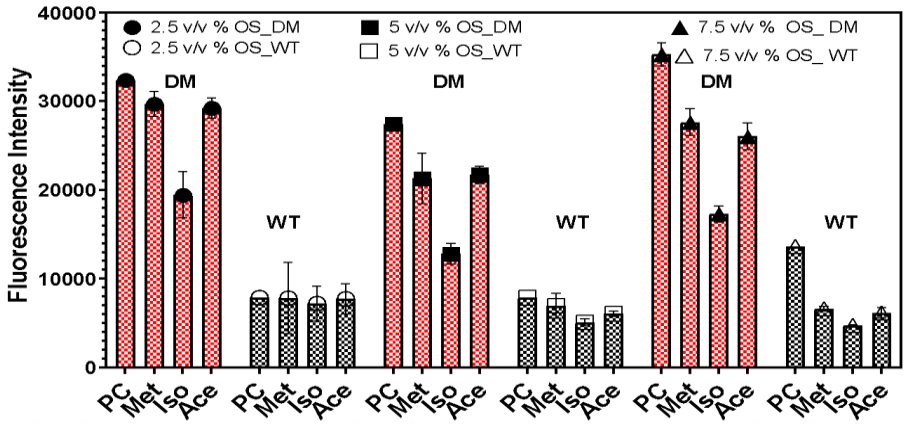

Figure 3.13 Screening of organic solvent effect were analyzed on peroxidation activity of WT CYP119(black) and T213R/T214I CYP119 (red). Reaction involved were .variable concentration (2.5, 5, 7.5) % v/v methanol, isopropanol and acetonitrile , 1.5 µM WT CYP119 and T213R/T214I CYP119 , 1.5 mM H_2O_2 and 10 µM Amplex® Red. Positive control (PC; without organic solvent).

Furthermore, we report that WT CYP119 and T213R/T214I CYP119 demonstrate strong stability in the presence of %2.5 v/v organic solvents (methanol, acetonitrile and isopropanol). However, other CYPs does not show high stability even in low concentrations of organic solvents.

3.8 Peroxidation Activity of WT CYP119 and T213R/T214I CYP119 based at variable pH

Investigations of Amplex Red peroxidation activity WT CYP119 and T213R/T214I CYP119 with variable pHs (5.8, 6.8, 7.4 ,8) in the presence of H_2O_2.. Amount of resorufin product formation is measured by using its extinction coefficient at 570 nm. Resorufin formation of WT CYP119 and T213R/T214I CYP119 was shown in Figure 3.14A and Figure 3.14B. Initial rate of resorufin formation was calculated by linear fitting. Relative activity of WT CYP119 and T213R/T214I CYP119 were drawn based on initial rate. The lowest peroxidation activity for WT CYP119 and T213R/T214I CYP119 was observed at pH 5.8. Peroxidation activity of the WT CYP119 increases at higher pH; our data shows similar results with literature. CYP119 displayed no reactivity nearly. However, this constantly increased upon raising the pH towards pH 8.5. (Rabe et

al., 2008). Peroxidation activity of WT CYP119 increases with increasing pH in the pH range tested. The highest peroxidation activity of WT CYP119 was tested at pH 8. On the other hand, peroxidation activity of T213R/T214I CYP119 demonstrates similar results at pH 6.8, 7.4 and 8 (Figure. 3.14A, Figure 3.14B). In acidic pH, T213R/T214I mutant shows higher peroxidation activity than WT CYP119 (Figure 3.14D). The highest peroxidation activity of T213R/T214I CYP119 was tested at pH 6.8.

Comparison of WT CYP119 and T213R/T213I demonstrates that the pH profile of CYP119 peroxidation activity changed with T213R/T214I mutation (Figure 3.14A, Figure 14B and Figure 3.14C). While WT CYP119 shows maximum peroxidation activity at pH 8, T213R/T213I CYP119 shows maximum peroxidation activity at pH 6.8 (Figure 3.14 D). Thus, T213R/T214I mutation of CYP119 altered the protonation state of the active site.

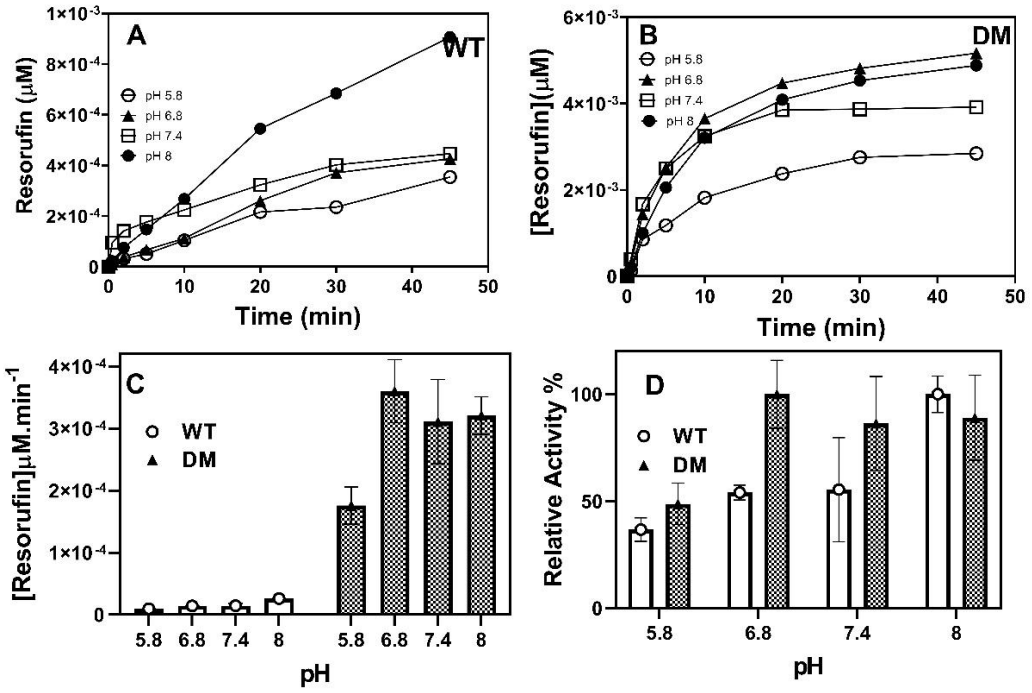

Figure 3.14 Resorufin formation in the presence of WT CYP119 (A) and T213R/T214I CYP119(B) at various pH values are illustrated. Initial rate of Amplex® Red peroxidation on different pHs are shown. The initial rate of Amplex® Red (10 μM) oxidation catalyzed by WT CYP119 and T213R/T214I CYP119 (1.5 μM) in the presence of H_2O_2 (1.5 mM) in 50 mM potassium phosphate buffer variable pHs (5.8, 6.8, 7.5, and 8.0) (C). Relative Activity of WT CYP119 and T213R/T214I CYP119 were shown (D).

3.9 Investigations of Temperature Stability of WT CYP119 and T213R/T214I CYP119

Temperature stability of WT CYP119 and T213R/T214I CYP119 were investigated. WT CYP119 (3.5 μM) and T213R/T214I (3.5 μM) in 50 mM potassium phosphate buffer were incubated for 5 minutes for each temperature in dry bath.

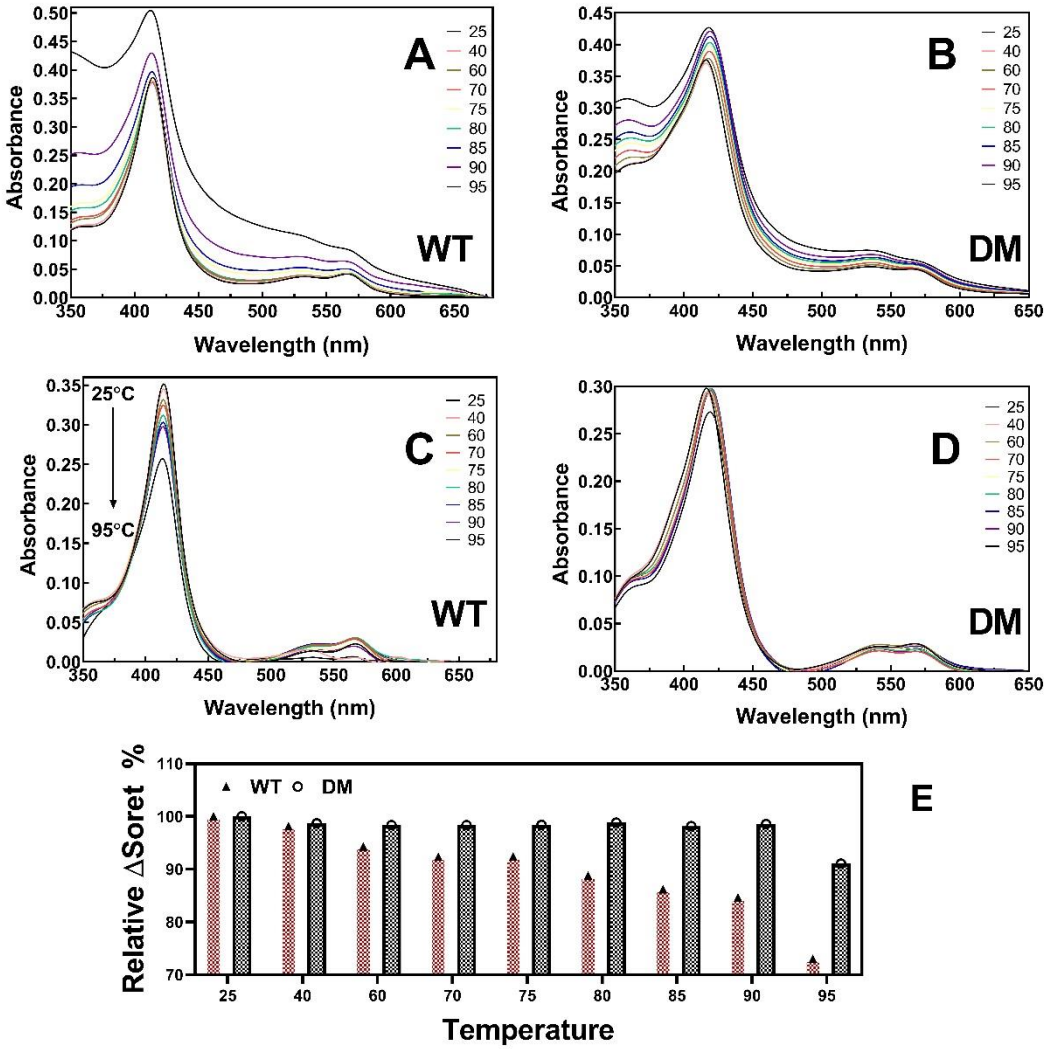

Figure 3.15 UV-Visible spectra of thermostability analysis of raw data of 3.5 μM WT CYP119 (A) and subtract data of WT CYP119 (B) were shown. UV-Visible spectra of thermostability analysis of raw data of 3.5 μM T213R/T214I CYP119 (C) and subtract data of T213R/T214I CYP119 (D) were shown. Change of Relative ΔSoret % of WT CYP119 (3.5 μM) and T213R/T214I CYP119 (3.5 μM) were illustrated for variable temperature (25, 40, 60, 70, 75, 80, 85, 90 and 95º C (E).

Figure 3.15C was obtained after background subtraction. When the applied temperature increases, decreases of maximum Soret absorbance of WT CYP119 was observed because of denaturation of apoprotein. When increased temperature effects on T213R/T214I CYP119 were analyzed, shift of maximum Soret absorbance was observed from 417 nm to 420 nm. Decreases of Soret absorbance of T213R/T214I CYP119 was seen at 95°C (Figure 3.15D). Relative Soret absorbance of WT CYP119 decreases with increasing of temperature as seen in Figure 3.15E. Previous studies have shown that Thr213 and Thr214 residues do not have a significant effect on thermal stability [2]. Increased temperatures may cause aggregation of apoprotein of WT CYP119 and T213R/T214I CYP119. (Figure 3.15A and Figure 3.15B). Comparison of relative Soret absorbance of T213R/T214I CYP119 and WT CYP119 demonstrate that T213R/T214I CYP119 is more stable towards increased temperatures compare to WT CYP119. Although, it was not expected alteration of thermal stability of CYP119 by mutation on Thr213 and Thr214, T213R/T214I CYP119 is stable compare to WT CYP119. To understand reason of thermal stability of T213R/T214I CYP119, further analysis should be performed.

3.10 Molecular Modelling and Docking of Different Substrates

Different ligands in in Table1 were docked into WT CYP119 (PDB ID: 1F4T) and T213R/T214I CYP119 by using the Pyrosetta program [58]. The lowest REU scores are demonstrated in Table 1.

Table 1 Docking energy scores of substrates were illustrated for WT CYP119 (1F4T) and T213R/T214I CYP119

Substrate	**WT CYP119 (REU)**	**T213R/T214I (REU)**
Caffeine	-418	-1195
Testesterone	-516	-1176
Progesterone	-412	-1119
Amplex®Red	-517	-1185
Guaiacol	-441	-1205
Phenoxazine	-528	-1209
Indole	-409	-1207
Indoxyl Acetate	-446	-1149
SDS	-441	-1178

After docking of ligands, investigations of location of the ligand, whether it was closer to the heme group or not, was investigated. Amplex® Red was closer to the heme group in T213R/T214I CYP119 compared to WT CYP119 as seen in Figure 3.16. Amplex® Red, Guaiacol, Progesterone, Testosterone, Caffeine, SDS , Indole and Indoxyl acetate and phenoxazine of 100 rounds of docking were performed for WT CYP119 and T213R/T214I CYP119. Scoring function of Pyrosetta occurs in a composition of physics based and knowledge-based information about the structure, thus the energy scores were calculated as a generic unit (REU). When the docking models were examined, the most negative REU scores were approved as more native-like [59]. The lowest REU scores were chosen to determine ligand-protein interactions.

Docking of Amplex® Red with WT CYP119 and T213R/T214I CYP119 shows that the lowest REU score of Amplex® Red with WT CYP119 which are -517 REU and T213R/T214I CYP119 which is -1185 REU. Obtained structure from docking studies indicates that Amplex® Red was closer to the heme group in T213R/T214I CYP119 (6.26 Å) compared to WT CYP119 (6.57 Å) in Figure 3.16. T213R/T214 CYP119 shows higher activity compare to WT CYP119 so that docking studies were performed to test for alterations in affinity for Amplex®Red. Actually, docking results showed lower binding energy, so that increased affinity for Amplex® Red for the improved variant.

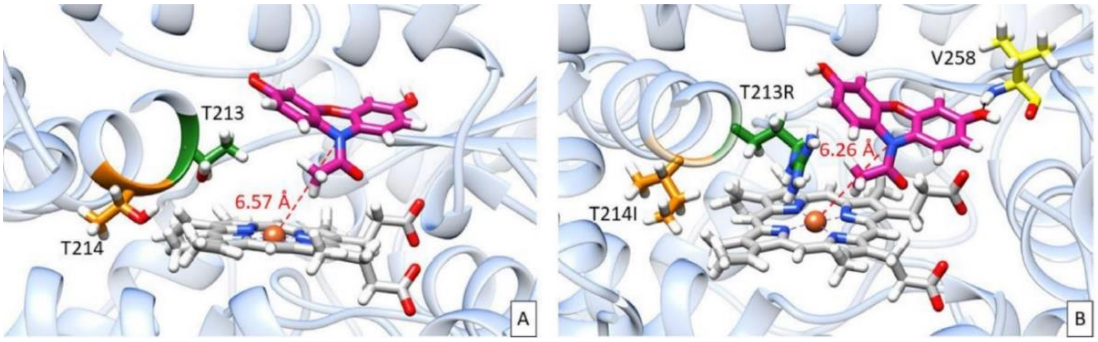

Figure 3.16 Docking studies of Amplex® Red (magenta) with WT CYP119 (PDB ID: 1F4T) and T213R/T214I CYP119 are seen that (A) WT CYP119 with Amplex® Red. Thr213 (green) and Thr214 (orange) residues are marked. Distance was labeled as 6.57 Å between heme iron and substrate (B) T213R/T214I CYP119 with Amplex® Red. Mutant residues are marked as T213R (green) and T214I (orange). Distance was labeled as Å between heme iron and substrate.

Docking of guaiacol with WT CYP119 and T213R/T214I CYP119 shows that the lowest REU score of guaiacol with WT CYP119 which are -441 REU and T213R/T214I CYP119 which is -1205 REU. Obtained structure from docking studies indicates that

guaiacol was closer to the heme group in T213R/T214I CYP119 (3.57 Å) compared to WT CYP119 (4.5 Å) in Figure 3.17. T213R/T214 CYP119 shows higher activity with guaiacol compared to WT CYP119. so that docking studies were performed to test for alterations in affinity for guaiacol. Indeed, docking results showed lower binding energy, so that increased affinity for guaiacol for the improved variant.

The lowest REU score of progesterone with WT CYP119 which is -412 REU. T213R/T214I CYP119 which is -1119 REU in Table 1. The distance between heme iron atom of CYPs and progesterone were measured. The distances were determined as 2.5 Å, for WT CYP119 and 2.4 Å for T231R/T214I mutant respectively. The progesterone is closer to the heme group in T213R/T214I CYP119 in contrast to WT CYP119 in Figure 3.18 so that progesterone binding studies of WT CYP119 and T213R/T214I CYP119 were performed to test for confirmed alterations in affinity for progesterone. Progesterone binding studies of WT CYP119 and T213R/T214I CYP119 demonstrate that T213R/T214I CYP119 shows higher affinity for progesterone compare to WT CYP119.

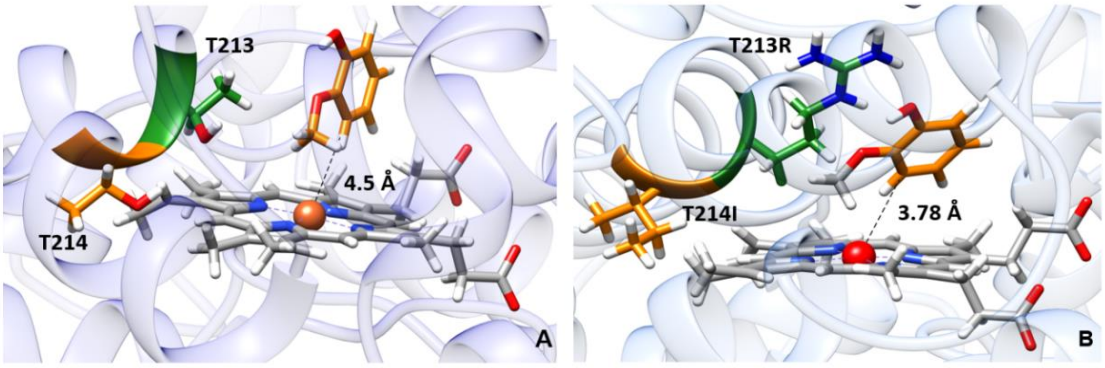

Figure 3.17 Docking studies of guaiacol (orange) with WT CYP119 (PDB ID: 1F4T) and T213R/T214I CYP119 are seen that (A) WT CYP119 with Guaiacol (orange), Thr213 (green) and Thr214 (orange) residues are marked. Distance was labeled as 4.5 Å between heme iron and substrate (B) T213R/T214I CYP119 with guaiacol. Mutant residues are marked as T213R (green) and T214I (orange). Distance was labeled as 3.78 Å between heme iron and closest carbon atom of substrate.

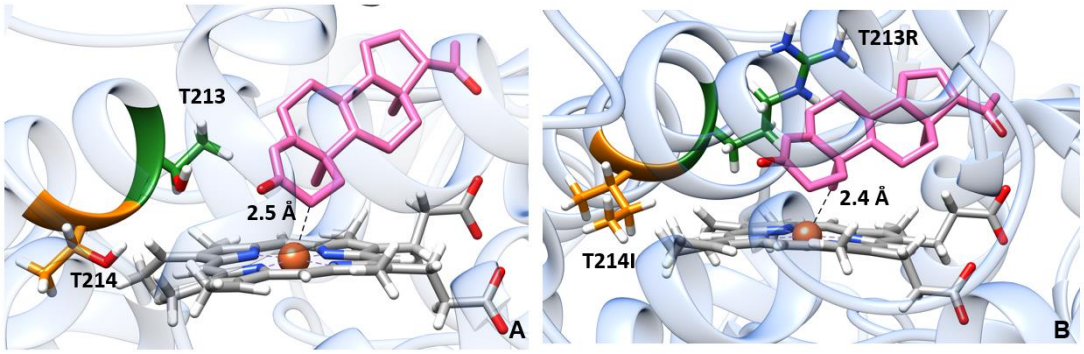

Figure 3.18 Docking studies of progesterone (pink) with WT CYP119 (PDB ID: 1F4T) and T213R/T214I CYP119 are seen that WT CYP119 (A) with progesterone. Thr213 (green) and Thr214 (orange) residues are marked. Distance was labeled as 2.5 Å between heme iron and substrate T213R/T214I CYP119 (B) with progesterone. Mutant residues are marked as T213R (green) and T214I (orange). Distance was labeled as 2.4 Å between heme iron and substrate.

CHAPTER 4

CONCLUSION

The novel T213R/T214I CYP119 is improved mutant that is obtained from Amplex® Red screening assay. As a result, T213R/T214I CYP119 demonstrated higher peroxidase activity for Amplex® Red, guaiacol and ABTS peroxidation and for styrene epoxidation. We report that T213R/T214I CYP119 shows 5-fold higher k_{cat} compared to WT CYP119 in the Amplex® Red peroxidation activity. Additionally, T213R/T214I CYP119 exhibited 2-fold higher k_{cat} for styrene epoxidation. Although, WT CYP119 demonstrates no peroxidase activity with guaiacol and ABTS in the presence of H_2O_2, T213R/T214I CYP119 shows interestingly peroxidase activity with guaiacol and ABTS in the presence of H_2O_2. Also, heme iron in T213R/T214I CYP119 shows high stability compare to WT CYP119 in the presence of peroxides which causes heme degradation in P450s. When binding studies of lauric acid and progesterone for WT CYP119 and T213R/T214I CYP119 were examined, T213R/T214I has 4-fold lower affinity for lauric acid and 10-fold higher affinity for progesterone compared to WT CYP119. On the other hand, when stabilities of WT CYP119 and T213R/T214I CYP119 were examined in terms of degradation in the presence of peroxides, temperature, pH and organic solvents, T213R/T214I CYP119 was more stable than WT CYP119. Furthermore, docking results show that mutations on Thr213 and Thr214 residues in the active site of CYP119 expands the substrate selectivity of WT CYP119. Characterization of T213R/T214I CYP119 illustrates higher stability than WT CYP119 in terms of variable temperature, pH and different organic solvent conditions. This novel mutant of CYP119 has a lot of potential for a cost-effective biocatalyst in industrial applications. T213R/T214I mutations on the active site provide an insight for the creation of new biocatalyst.

REFERENCES

(1) Kaushik, M.; Sinha, P.; Jaiswal, P.; Mahendru, S.; Roy, K.; Kukreti, S. Protein Engineering and de Novo Designing of a Biocatalyst. *Journal of molecular recognition : JMR*. 2016. https://doi.org/10.1002/jmr.2546.

(2) Koo, L. S.; Tschirret-Guth, R. A.; Straub, W. E.; Moënne-Loccoz, P.; Loehr, T. M.; Ortiz De Montellano, P. R. The Active Site of the Thermophilic CYP119 from Sulfolobus Solfataricus. *J. Biol. Chem.* **2000**, *275* (19), 14112–14123. https://doi.org/10.1074/jbc.275.19.14112.

(3) McAuliffe, J. C. Industrial Enzymes and Biocatalysis. In *Handbook of Industrial Chemistry and Biotechnology: Twelfth Edition*; 2012. https://doi.org/10.1007/978-1-4614-4259-2_31.

(4) Osbon, Y.; Kumar, M. Biocatalysis and Strategies for Enzyme Improvement. In *Biophysical Chemistry - Advance Applications*; 2020. https://doi.org/10.5772/intechopen.85018.

(5) Turanli-Yildiz, B.; Alkim, C.; Petek, Z. Protein Engineering Methods and Applications. In *Protein Engineering*; 2012. https://doi.org/10.5772/27306.

(6) Ẅiderek, K.; Tuñón, I.; Moliner, V.; Bertran, J. Computational Strategies for the Design of New Enzymatic Functions. *Archives of Biochemistry and Biophysics*. 2015. https://doi.org/10.1016/j.abb.2015.03.013.

(7) Woolfson, D. N.; Bartlett, G. J.; Burton, A. J.; Heal, J. W.; Niitsu, A.; Thomson, A. R.; Wood, C. W. De Novo Protein Design: How Do We Expand into the Universe of Possible Protein Structures? *Current Opinion in Structural Biology*. 2015. https://doi.org/10.1016/j.sbi.2015.05.009.

(8) Díaz-Rodríguez, A.; Davis, B. G. Chemical Modification in the Creation of Novel Biocatalysts. *Current Opinion in Chemical Biology*. 2011. https://doi.org/10.1016/j.cbpa.2010.12.002.

(9) O'Reilly, E.; Köhler, V.; Flitsch, S. L. Cytochromes P450 as Useful Biocatalysts: Addressing the Limitations. *Chem. Commun.* **2011**. https://doi.org/10.1039/c0cc03165h.

(10) Bommarius, A. S.; Blum, J. K.; Abrahamson, M. J. Status of Protein Engineering for Biocatalysts: How to Design an Industrially Useful Biocatalyst. *Current Opinion in Chemical Biology*. 2011. https://doi.org/10.1016/j.cbpa.2010.11.011.

(11) Bommarius, A. S.; Paye, M. F. Stabilizing Biocatalysts. *Chem. Soc. Rev.* **2013**. https://doi.org/10.1039/c3cs60137d.

(12) Hibbert, E. G.; Dalby, P. A. Directed Evolution Strategies for Improved Enzymatic Performance. *Microbial Cell Factories*. 2005. https://doi.org/10.1186/1475-2859-

4-29.

(13) Arnold, F. H.; Wintrode, P. L.; Miyazaki, K.; Gershenson, A. How Enzymes Adapt: Lessons from Directed Evolution. *Trends in Biochemical Sciences*. 2001. https://doi.org/10.1016/S0968-0004(00)01755-2.

(14) Bornscheuer, U. T.; Pohl, M. Improved Biocatalysts by Directed Evolution and Rational Protein Design. *Current Opinion in Chemical Biology*. 2001. https://doi.org/10.1016/S1367-5931(00)00182-4.

(15) Urlacher, V. B.; Lutz-Wahl, S.; Schmid, R. D. Microbial P450 Enzymes in Biotechnology. *Applied Microbiology and Biotechnology*. 2004. https://doi.org/10.1007/s00253-003-1514-1.

(16) Rabe, K. S.; Kiko, K.; Niemeyer, C. M. Characterization of the Peroxidase Activity of CYP119, a Thermostable P450 from Sulfolobus Acidocaldarius. *ChemBioChem* **2008**, *9* (3), 420–425. https://doi.org/10.1002/cbic.200700450.

(17) McLean, M. A.; Maves, S. A.; Weiss, K. E.; Krepich, S.; Sligar, S. G. Characterization of a Cytochrome P450 from the Acidothermophilic ArchaeaSulfolobus Solfataricus. *Biochem. Biophys. Res. Commun.* **1998**, *252* (1), 166–172. https://doi.org/10.1006/bbrc.1998.9584.

(18) Jung, S. T.; Lauchli, R.; Arnold, F. H. Cytochrome P450: Taming a Wild Type Enzyme. *Current Opinion in Biotechnology*. 2011. https://doi.org/10.1016/j.copbio.2011.02.008.

(19) Denisov, I. G.; Makris, T. M.; Sligar, S. G.; Schlichting, I. Structure and Chemistry of Cytochrome P450. *Chemical Reviews*. 2005. https://doi.org/10.1021/cr0307143.

(20) Anderson, J. L. R.; Chapman, S. K. Ligand Probes for Heme Proteins. *Dalton Transactions*. 2005. https://doi.org/10.1039/b413046d.

(21) McLean, K. J.; Sabri, M.; Marshall, K. R.; Lawson, R. J.; Lewis, D. G.; Clift, D.; Balding, P. R.; Dunford, A. J.; Warman, A. J.; McVey, J. P.; Quinn, A. M.; Sutcliffe, M. J.; Scrutton, N. S.; Munro, A. W. Biodiversity of Cytochrome P450 Redox Systems. In *Biochemical Society Transactions*; 2005. https://doi.org/10.1042/BST0330796.

(22) Hrycay, E. G.; Bandiera, S. M. Monooxygenase, Peroxidase and Peroxygenase Properties and Reaction Mechanisms of Cytochrome P450 Enzymes. *Adv. Exp. Med. Biol.* **2015**, *851*, 1–61. https://doi.org/10.1007/978-3-319-16009-2_1.

(23) McLean, M. A.; Maves, S. A.; Weiss, K. E.; Krepich, S.; Sligar, S. G. Characterization of a Cytochrome P450 from the Acidothermophilic Archaea Sulfolobus Solfataricus. *Biochem. Biophys. Res. Commun.* **1998**. https://doi.org/10.1006/bbrc.1998.9584.

(24) Omura, T. Recollection of the Early Years of the Research on Cytochrome P450.

Proceedings of the Japan Academy Series B: Physical and Biological Sciences. 2011. https://doi.org/10.2183/pjab.87.617.

(25) Bernhardt, R.; Urlacher, V. B. Cytochromes P450 as Promising Catalysts for Biotechnological Application: Chances and Limitations. *Applied Microbiology and Biotechnology*. 2014. https://doi.org/10.1007/s00253-014-5767-7.

(26) Bernhardt, R. Cytochromes P450 as Versatile Biocatalysts. *J. Biotechnol.* **2006**. https://doi.org/10.1016/j.jbiotec.2006.01.026.

(27) Munro, A. W.; Lindsay, J. G. Bacterial Cytochromes P-450. *Molecular Microbiology*. 1996. https://doi.org/10.1111/j.1365-2958.1996.tb02632.x.

(28) Waskell, L.; Kim, J. J. P. Electron Transfer Partners of Cytochrome P450. In *Cytochrome P450: Structure, Mechanism, and Biochemistry, Fourth Edition*; 2015. https://doi.org/10.1007/978-3-319-12108-6_2.

(29) Hannemann, F.; Bichet, A.; Ewen, K. M.; Bernhardt, R. Cytochrome P450 Systems-Biological Variations of Electron Transport Chains. *Biochimica et Biophysica Acta - General Subjects*. 2007. https://doi.org/10.1016/j.bbagen.2006.07.017.

(30) Munro, A. W.; Mclean, K. J.; Grant, J. L.; Makris, T. M. Structure and Function of the Cytochrome P450 Peroxygenase Enzymes. **2018**. https://doi.org/10.1042/BST20170218.

(31) Zanger, U. M.; Schwab, M. Cytochrome P450 Enzymes in Drug Metabolism: Regulation of Gene Expression, Enzyme Activities, and Impact of Genetic Variation. *Pharmacology and Therapeutics*. 2013. https://doi.org/10.1016/j.pharmthera.2012.12.007.

(32) Vieille, C.; Zeikus, G. J. Hyperthermophilic Enzymes: Sources, Uses, and Molecular Mechanisms for Thermostability. *Microbiol. Mol. Biol. Rev.* **2001**. https://doi.org/10.1128/mmbr.65.1.1-43.2001.

(33) Wright, R. L.; Harris, K.; Solow, B.; White, R. H.; Kennelly, P. J. Cloning of a Potential Cytochrome P450 from the Archaeon Sulfolobus Solfataricus. *FEBS Lett.* **1996**. https://doi.org/10.1016/0014-5793(96)00322-5.

(34) Salazar, O.; Cirino, P. C.; Arnold, F. H. Thermostabilization of a Cytochrome P450 Peroxygenase. *ChemBioChem* **2003**. https://doi.org/10.1002/cbic.200300660.

(35) Cirino, P. C.; Arnold, F. H. Protein Engineering of Oxygenases for Biocatalysis. *Current Opinion in Chemical Biology*. 2002. https://doi.org/10.1016/S1367-5931(02)00305-8.

(36) Liu, Z.; Lemmonds, S.; Huang, J.; Tyagi, M.; Hong, L.; Jain, N. Entropic Contribution to Enhanced Thermal Stability in the Thermostable P450 CYP119. *Proc. Natl. Acad. Sci. U. S. A.* **2018**. https://doi.org/10.1073/pnas.1807473115.

(37) Stepankova, V.; Bidmanova, S.; Koudelakova, T.; Prokop, Z.; Chaloupkova, R.; Damborsky, J. Strategies for Stabilization of Enzymes in Organic Solvents. *ACS Catalysis*. 2013. https://doi.org/10.1021/cs400684x.

(38) Brock, T. D.; Brock, K. M.; Belly, R. T.; Weiss, R. L. Sulfolobus: A New Genus of Sulfur-Oxidizing Bacteria Living at Low PH and High Temperature. *Arch. Mikrobiol.* **1972**. https://doi.org/10.1007/BF00408082.

(39) de Montellano, P. R. O. *Cytochrome P450: Structure, Mechanism, and Biochemistry, Fourth Edition*; 2015. https://doi.org/10.1007/978-3-319-12108-6.

(40) Poulos, T. L.; Johnson, E. F. Structures of Cytochrome P450 Enzymes. In *Cytochrome P450: Structure, Mechanism, and Biochemistry, Fourth Edition*; 2015. https://doi.org/10.1007/978-3-319-12108-6_1.

(41) Yano, J. K.; Koo, L. S.; Schuller, D. J.; Li, H.; Ortiz de Montellano, P. R.; Poulos, T. L. Crystal Structure of a Thermophilic Cytochrome P450 from the Archaeon Sulfolobus Solfataricus*. **2000**. https://doi.org/10.1074/jbc.M004281200.

(42) Park, S. Y.; Yamane, K.; Adachi, S. I.; Shiro, Y.; Weiss, K. E.; Maves, S. A.; Sligar, S. G. Thermophilic Cytochrome P450 (CYP119) from Sulfolobus Solfataricus: High Resolution Structure and Functional Properties. *J. Inorg. Biochem.* **2002**, *91* (4), 491–501. https://doi.org/10.1016/S0162-0134(02)00446-4.

(43) MARDEN, M. C.; Hui bon hoa, G. Dynamics of the Spin Transition in Camphor-Bound Ferric Cytochrome P-450 versus Temperature, Pressure and Viscosity. *Eur. J. Biochem.* **1982**. https://doi.org/10.1111/j.1432-1033.1982.tb07028.x.

(44) Sligar, S. G. Coupling of Spin, Substrate, and Redox Equilibriums in Cytochrome P450. *Biochemistry* **1976**. https://doi.org/10.1021/bi00669a029.

(45) Nishida, C. R.; Ortiz De Montellano, P. R. Thermophilic Cytochrome P450 Enzymes. *Biochemical and Biophysical Research Communications*. 2005. https://doi.org/10.1016/j.bbrc.2005.08.093.

(46) Yano, J. K.; Blasco, F.; Li, H.; Schmid, R. D.; Henne, A.; Poulos, T. L. Preliminary Characterization and Crystal Structure of a Thermostable Cytochrome P450 from Thermus Thermophilus. *J. Biol. Chem.* **2003**. https://doi.org/10.1074/jbc.M206568200.

(47) Rabe, K. S.; Kiko, K.; Niemeyer, C. M. Characterization of the Peroxidase Activity of CYP119, a Thermostable P450 FromSulfolobus Acidocaldarius. *ChemBioChem* **2008**, *9* (3), 420–425. https://doi.org/10.1002/cbic.200700450.

(48) Rabe, K. S.; Gandubert, V. J.; Spengler, M.; Erkelenz, M.; Niemeyer, C. M. Engineering and Assaying of Cytochrome P450 Biocatalysts. *Analytical and Bioanalytical Chemistry*. 2008. https://doi.org/10.1007/s00216-008-2248-9.

(49) Aslantas, Y.; Surmeli, N. B. Effects of N-Terminal and C-Terminal Polyhistidine Tag on the Stability and Function of the Thermophilic P450 CYP119. *Bioinorg.*

Chem. Appl. **2019**, *2019*. https://doi.org/10.1155/2019/8080697.

(50) Başlar, M. S.; Sakallı, T.; Güralp, G.; Kestevur Doğru, E.; Haklı, E.; Surmeli, N. B. Development of an Improved Amplex Red Peroxidation Activity Assay for Screening Cytochrome P450 Variants and Identification of a Novel Mutant of the Thermophilic CYP119. *J. Biol. Inorg. Chem.* **2020**. https://doi.org/10.1007/s00775-020-01816-w.

(51) Sharma, P.; Jha, A. B.; Dubey, R. S.; Pessarakli, M. Reactive Oxygen Species, Oxidative Damage, and Antioxidative Defense Mechanism in Plants under Stressful Conditions. *J. Bot.* **2012**, *2012*, 1–26. https://doi.org/10.1155/2012/217037.

(52) Koduri, R. S.; Tien, M. *Oxidation of Guaiacol by Lignin Peroxidase ROLE OF VERATRYL ALCOHOL**; 1995.

(53) Doerge, D. R.; Divi, R. L.; Churchwell, M. I. Identification of the Colored Guaiacol Oxidation Product Produced by Peroxidases. *Anal. Biochem.* **1997**. https://doi.org/10.1006/abio.1997.2191.

(54) Aggrey-Fynn, J. E.; Surmeli, N. B. A Novel Thermophilic Hemoprotein Scaffold for Rational Design of Biocatalysts. *J. Biol. Inorg. Chem.* **2018**, *23* (8), 1295–1307. https://doi.org/10.1007/s00775-018-1615-z.

(55) Koo, L. S.; Immoos, C. E.; Cohen, M. S.; Farmer, P. J.; Ortiz de Montellano, P. R. Enhanced Electron Transfer and Lauric Acid Hydroxylation by Site-Directed Mutagenesis of CYP119. *J. Am. Chem. Soc.* **2002**. https://doi.org/10.1021/ja017174g.

(56) Reetz, M. T.; Bocola, M.; Carballeira, J. D.; Zha, D.; Vogel, A. Expanding the Range of Substrate Acceptance of Enzymes: Combinatorial Active-Site Saturation Test. *Angew. Chemie - Int. Ed.* **2005**. https://doi.org/10.1002/anie.200500767.

(57) Shoji, O.; Watanabe, Y. Peroxygenase Reactions Catalyzed by Cytochromes P450. *JBIC J. Biol. Inorg. Chem.* **2014**. https://doi.org/10.1007/s00775-014-1106-9.

(58) Chaudhury, S.; Lyskov, S.; Gray, J. J. PyRosetta: A Script-Based Interface for Implementing Molecular Modeling Algorithms Using Rosetta. *Bioinformatics* **2010**, *26* (5), 689–691. https://doi.org/10.1093/bioinformatics/btq007.

(59) Misura, K. M. S.; Chivian, D.; Rohl, C. A.; Kim, D. E.; Baker, D. Physically Realistic Homology Models Built with ROSETTA Can Be More Accurate than Their Templates. *Proc. Natl. Acad. Sci. U. S. A.* **2006**. https://doi.org/10.1073/pnas.0509355103.

APPENDIX A

```
from rosetta import *
from toolbox import *
from rosetta.protocols.rigid import *
from rosetta.protocols.ligand_docking import *
init()

import os


pose = pose_from_pdb("C:\Users\Public\\1F4T.pdb")

scorefxn = create_score_function("ref2015")

outfile = open(r"C:\Users\Public\Desktop\1F4T_LIGAND_NAME.txt","a")

from rosetta.protocols.relax import *
relax = FastRelax()
relax.set_scorefxn(scorefxn)


outfile.write("Native energy of wild type protein = %f\r\n" % scorefxn(pose))



outfile.close()



pose_list = ["1F4T"]
```

```
for v in pose_list:
    with open(r"C:\Users\Public\\" + str(v) + ".pdb", "r+") as f:
        new_f = f.readlines()
        f.seek(0)
        for line in new_f:
            if "HETATM" not in line:
                f.write(line)
        f.truncate()
    output = open(r"C:\Users\Public\\" + str(v) + ".pdb", "a")
    output.write("""
```

LIGAND

```
HETATM    1  C1  hem X   1      58.435  17.806  15.041  1.00 20.00           C
HETATM    2  C2  hem X   1      54.889  19.461  17.930  1.00 20.00           C
HETATM    3  C3  hem X   1      55.661  23.971  16.283  1.00 20.00           C
HETATM    4  C4  hem X   1      58.792  22.213  13.083  1.00 20.00           C
HETATM    5  C5  hem X   1      57.463  17.884  16.047  1.00 20.00           C
HETATM    6  C6  hem X   1      57.005  16.748  16.809  1.00 20.00           C
HETATM    7  C7  hem X   1      55.982  17.210  17.603  1.00 20.00           C
HETATM    8  C8  hem X   1      55.831  18.610  17.315  1.00 20.00           C
HETATM    9  C9  hem X   1      55.183  16.402  18.633  1.00 20.00           C
HETATM   10  C10 hem X   1      57.558  15.324  16.699  1.00 20.00           C
HETATM   11  C11 hem X   1      56.545  14.355  16.053  1.00 20.00           C
HETATM   12  C12 hem X   1      57.070  12.932  15.923  1.00 20.00           C
HETATM   13  O1  hem X   1      57.980  12.555  16.692  1.00 20.00           O
HETATM   14  O2  hem X   1      56.550  12.176  15.065  1.00 20.00           O
HETATM   15  C13 hem X   1      54.768  20.833  17.694  1.00 20.00           C
HETATM   16  C14 hem X   1      53.964  21.714  18.504  1.00 20.00           C
HETATM   17  C15 hem X   1      54.157  22.977  18.032  1.00 20.00           C
HETATM   18  C16 hem X   1      55.141  22.862  16.975  1.00 20.00           C
HETATM   19  C17 hem X   1      53.152  21.317  19.734  1.00 20.00           C
HETATM   20  C18 hem X   1      53.491  24.150  18.374  1.00 20.00           C
HETATM   21  C19 hem X   1      53.246  24.596  19.742  1.00 20.00           C
```

```
HETATM   22  C20 hem X   1      56.608  23.887  15.273  1.00 20.00           C
HETATM   23  C21 hem X   1      57.162  25.026  14.538  1.00 20.00           C
HETATM   24  C22 hem X   1      57.977  24.502  13.559  1.00 20.00           C
HETATM   25  C23 hem X   1      57.984  23.085  13.783  1.00 20.00           C
HETATM   26  C24 hem X   1      56.947  26.504  14.897  1.00 20.00           C
HETATM   27  C25 hem X   1      58.678  25.123  12.512  1.00 20.00           C
HETATM   28  C26 hem X   1      58.502  26.463  12.049  1.00 20.00           C
HETATM   29  C27 hem X   1      58.935  20.861  13.343  1.00 20.00           C
HETATM   30  C28 hem X   1      59.786  20.007  12.550  1.00 20.00           C
HETATM   31  C29 hem X   1      59.764  18.802  13.149  1.00 20.00           C
HETATM   32  C30 hem X   1      58.832  18.890  14.252  1.00 20.00           C
HETATM   33  C31 hem X   1      60.572  20.378  11.286  1.00 20.00           C
HETATM   34  C32 hem X   1      60.594  17.625  12.699  1.00 20.00           C
HETATM   35  C33 hem X   1      61.724  17.254  13.643  1.00 20.00           C
HETATM   36  C34 hem X   1      62.412  15.976  13.233  1.00 20.00           C
HETATM   37  O3  hem X   1      61.745  15.109  12.615  1.00 20.00           O
HETATM   38  O4  hem X   1      63.615  15.826  13.536  1.00 20.00           O
HETATM   39  N1  hem X   1      56.737  19.024  16.350  1.00 20.00           N
HETATM   40  N2  hem X   1      55.505  21.543  16.761  1.00 20.00           N
HETATM   41  N3  hem X   1      57.129  22.691  14.808  1.00 20.00           N
HETATM   42  N4  hem X   1      58.298  20.177  14.349  1.00 20.00           N
HETATM   43 FE1  hem X   1      56.853  20.817  15.518  1.00 20.00          FE
HETATM   44  H1  hem X   1      58.906  16.851  14.864  1.00 20.00           H
HETATM   45  H2  hem X   1      54.207  19.017  18.640  1.00 20.00           H
HETATM   46  H3  hem X   1      55.299  24.951  16.556  1.00 20.00           H
HETATM   47  H4  hem X   1      59.362  22.620  12.261  1.00 20.00           H
HETATM   48  H5  hem X   1      58.462  15.344  16.090  1.00 20.00           H
HETATM   49  H6  hem X   1      57.809  14.963  17.696  1.00 20.00           H
HETATM   50  H7  hem X   1      56.299  14.725  15.058  1.00 20.00           H
HETATM   51  H8  hem X   1      55.638  14.341  16.657  1.00 20.00           H
HETATM   52  H9  hem X   1      53.130  24.775  17.570  1.00 20.00           H
HETATM   53  H10 hem X   1      59.424  24.528  12.007  1.00 20.00           H
HETATM   54  H11 hem X   1      61.027  17.865  11.728  1.00 20.00           H
HETATM   55  H12 hem X   1      59.939  16.761  12.584  1.00 20.00           H
```

```
HETATM   56  H13 hem X   1      62.457  18.061  13.648  1.00 20.00           H
HETATM   57  H14 hem X   1      61.322  17.134  14.649  1.00 20.00           H
HETATM   58  H15 hem X   1      54.456  17.052  19.121  1.00 20.00           H
HETATM   59  H16 hem X   1      54.662  15.588  18.130  1.00 20.00           H
HETATM   60  H17 hem X   1      55.863  15.992  19.380  1.00 20.00           H
HETATM   61  H18 hem X   1      58.989  26.580  11.081  1.00 20.00           H
HETATM   62  H19 hem X   1      58.945  27.155  12.765  1.00 20.00           H
HETATM   63  H20 hem X   1      57.438  26.676  11.949  1.00 20.00           H
HETATM   64  H21 hem X   1      53.083  20.231  19.789  1.00 20.00           H
HETATM   65  H22 hem X   1      52.151  21.741  19.660  1.00 20.00           H
HETATM   66  H23 hem X   1      53.642  21.696  20.631  1.00 20.00           H
HETATM   67  H24 hem X   1      56.425  26.574  15.851  1.00 20.00           H
HETATM   68  H25 hem X   1      56.350  26.983  14.121  1.00 20.00           H
HETATM   69  H26 hem X   1      57.913  27.004  14.973  1.00 20.00           H
HETATM   70  H27 hem X   1      60.367  21.415  11.021  1.00 20.00           H
HETATM   71  H28 hem X   1      61.639  20.255  11.473  1.00 20.00           H
HETATM   72  H29 hem X   1      60.269  19.727  10.466  1.00 20.00           H
HETATM   73  H30 hem X   1      53.271  25.685  19.780  1.00 20.00           H
HETATM   74  H31 hem X   1      54.017  24.192  20.399  1.00 20.00           H
HETATM   75  H32 hem X   1      52.268  24.243  20.070  1.00 20.00           H
""")
    output.close()


output = open(r"C:\Users\Public\Desktop\1F4T_LIGAND_NAME.txt","a")
output.write("DOCKING RESULTS FOR AXR \n")
scorefxn = create_score_function("ligand")
docking = DockMCMProtocol()
docking.set_scorefxn(scorefxn)

params_list = Vector1(["LIGAND_NAME.params"])
res_set = generate_nonstandard_residue_set(params_list)

for i in pose_list:
```

```
    v ="C:\Users\Public\\"+ str(i) + ".pdb"
    pose = Pose()
    pose_from_pdb(pose,res_set, str(v))
    job_output = str(i) + "_dao"
    jd = PyJobDistributor(job_output, 100, scorefxn)
    test_pose = Pose()
    counter = 0
    while not jd.job_complete:
        test_pose.assign(pose)
        counter += 1
        test_pose.pdb_info().name(job_output + '_' + str(counter))
        docking.apply(test_pose)
        test_pose.pdb_info().name(job_output + '_' + str(counter) + '_fa')
        jd.output_decoy(test_pose)

for i in pose_list:
    x = 1
    name ="C:\Users\Public\\"+ str(i) + ".pdb"
    output.write("*" * 102 + "\n")
    output.write("Docking results of model " + str(name) + "\n")
    for x in range(1,101):
        v = str(i) + "_dao_" + str(x) + ".pdb"
        pose = Pose()
        pose_from_pdb(pose, res_set, str(v))
        scr = int(scorefxn(pose))
        #if scr <= 0:
        output.write("Docking score " + str(x) + " = %f\r\n" % scr)
        #if scr >= 0:
            #os.remove(r"C:\Users\Public\\" + str(v))

output.close()
```

```
from rosetta import *
from toolbox import *
from rosetta.protocols.rigid import *
from rosetta.protocols.ligand_docking import *
init()

import os



pose = pose_from_pdb("C:\Users\Public\\T213R_T214I.pdb")

scorefxn = create_score_function("ref2015")

outfile =
open(r"C:\Users\Public\Desktop\T213R_T214I_LIGAND_NAME.txt","a")

from rosetta.protocols.relax import *
relax = FastRelax()
relax.set_scorefxn(scorefxn)

outfile.write("Native energy of wild type protein = %f\r\n" % scorefxn(pose))



outfile.close()



pose_list = ["T213R_T214I"]
for v in pose_list:
    with open(r"C:\Users\Public\\" + str(v) + ".pdb", "r+") as f:
        new_f = f.readlines()
```

```
            f.seek(0)
            for line in new_f:
               if "HETATM" not in line:
                  f.write(line)
            f.truncate()
         output = open(r"C:\Users\Public\\" + str(v) + ".pdb", "a")
         output.write("""HETATM    1  C1  RED X   1      52.429  15.176  13.678  1.00
20.00          C
        HETATM    2  C2  RED X   1      53.838  15.783  13.713  1.00 20.00          C
        HETATM    3  O1  RED X   1      54.787  15.030  13.845  1.00 20.00          O
        HETATM    4  N1  RED X   1      53.995  17.153  13.443  1.00 20.00          N
        HETATM    5  C3  RED X   1      52.910  18.042  13.138  1.00 20.00          C
        HETATM    6  C4  RED X   1      53.000  18.859  11.989  1.00 20.00          C
        HETATM    7  C5  RED X   1      51.933  19.691  11.612  1.00 20.00          C
        HETATM    8  C6  RED X   1      50.768  19.728  12.395  1.00 20.00          C
        HETATM    9  C7  RED X   1      50.696  18.975  13.581  1.00 20.00          C
        HETATM   10  C8  RED X   1      51.770  18.151  13.960  1.00 20.00          C
        HETATM   11  O2  RED X   1      54.183  18.903  11.284  1.00 20.00          O
        HETATM   12  C9  RED X   1      55.346  18.515  11.916  1.00 20.00          C
        HETATM   13  C10 RED X   1      55.271  17.687  13.060  1.00 20.00          C
        HETATM   14  C11 RED X   1      56.459  17.392  13.762  1.00 20.00          C
        HETATM   15  C12 RED X   1      57.698  17.867  13.301  1.00 20.00          C
        HETATM   16  C13 RED X   1      57.762  18.659  12.142  1.00 20.00          C
        HETATM   17  C14 RED X   1      56.582  18.994  11.456  1.00 20.00          C
        HETATM   18  O3  RED X   1      58.962  19.119  11.688  1.00 20.00          O
        HETATM   19  H1  RED X   1      59.350  19.713  12.356  1.00 20.00          H
        HETATM   20  O4  RED X   1      49.726  20.526  12.022  1.00 20.00          O
        HETATM   21  H2  RED X   1      49.975  21.459  12.142  1.00 20.00          H
        TER
        HETATM    1  C1  hem X   1      58.435  17.806  15.041  1.00 20.00          C
        HETATM    2  C2  hem X   1      54.889  19.461  17.930  1.00 20.00          C
        HETATM    3  C3  hem X   1      55.661  23.971  16.283  1.00 20.00          C
        HETATM    4  C4  hem X   1      58.792  22.213  13.083  1.00 20.00          C
        HETATM    5  C5  hem X   1      57.463  17.884  16.047  1.00 20.00          C
```

```
HETATM    6  C6  hem X   1      57.005  16.748  16.809  1.00 20.00           C
HETATM    7  C7  hem X   1      55.982  17.210  17.603  1.00 20.00           C
HETATM    8  C8  hem X   1      55.831  18.610  17.315  1.00 20.00           C
HETATM    9  C9  hem X   1      55.183  16.402  18.633  1.00 20.00           C
HETATM   10  C10 hem X   1      57.558  15.324  16.699  1.00 20.00           C
HETATM   11  C11 hem X   1      56.545  14.355  16.053  1.00 20.00           C
HETATM   12  C12 hem X   1      57.070  12.932  15.923  1.00 20.00           C
HETATM   13  O1  hem X   1      57.980  12.555  16.692  1.00 20.00           O
HETATM   14  O2  hem X   1      56.550  12.176  15.065  1.00 20.00           O
HETATM   15  C13 hem X   1      54.768  20.833  17.694  1.00 20.00           C
HETATM   16  C14 hem X   1      53.964  21.714  18.504  1.00 20.00           C
HETATM   17  C15 hem X   1      54.157  22.977  18.032  1.00 20.00           C
HETATM   18  C16 hem X   1      55.141  22.862  16.975  1.00 20.00           C
HETATM   19  C17 hem X   1      53.152  21.317  19.734  1.00 20.00           C
HETATM   20  C18 hem X   1      53.491  24.150  18.374  1.00 20.00           C
HETATM   21  C19 hem X   1      53.246  24.596  19.742  1.00 20.00           C
HETATM   22  C20 hem X   1      56.608  23.887  15.273  1.00 20.00           C
HETATM   23  C21 hem X   1      57.162  25.026  14.538  1.00 20.00           C
HETATM   24  C22 hem X   1      57.977  24.502  13.559  1.00 20.00           C
HETATM   25  C23 hem X   1      57.984  23.085  13.783  1.00 20.00           C
HETATM   26  C24 hem X   1      56.947  26.504  14.897  1.00 20.00           C
HETATM   27  C25 hem X   1      58.678  25.123  12.512  1.00 20.00           C
HETATM   28  C26 hem X   1      58.502  26.463  12.049  1.00 20.00           C
HETATM   29  C27 hem X   1      58.935  20.861  13.343  1.00 20.00           C
HETATM   30  C28 hem X   1      59.786  20.007  12.550  1.00 20.00           C
HETATM   31  C29 hem X   1      59.764  18.802  13.149  1.00 20.00           C
HETATM   32  C30 hem X   1      58.832  18.890  14.252  1.00 20.00           C
HETATM   33  C31 hem X   1      60.572  20.378  11.286  1.00 20.00           C
HETATM   34  C32 hem X   1      60.594  17.625  12.699  1.00 20.00           C
HETATM   35  C33 hem X   1      61.724  17.254  13.643  1.00 20.00           C
HETATM   36  C34 hem X   1      62.412  15.976  13.233  1.00 20.00           C
HETATM   37  O3  hem X   1      61.745  15.109  12.615  1.00 20.00           O
HETATM   38  O4  hem X   1      63.615  15.826  13.536  1.00 20.00           O
HETATM   39  N1  hem X   1      56.737  19.024  16.350  1.00 20.00           N
```

HETATM 40 N2 hem X 1 55.505 21.543 16.761 1.00 20.00 N
HETATM 41 N3 hem X 1 57.129 22.691 14.808 1.00 20.00 N
HETATM 42 N4 hem X 1 58.298 20.177 14.349 1.00 20.00 N
HETATM 43 FE1 hem X 1 56.853 20.817 15.518 1.00 20.00 FE
HETATM 44 H1 hem X 1 58.906 16.851 14.864 1.00 20.00 H
HETATM 45 H2 hem X 1 54.207 19.017 18.640 1.00 20.00 H
HETATM 46 H3 hem X 1 55.299 24.951 16.556 1.00 20.00 H
HETATM 47 H4 hem X 1 59.362 22.620 12.261 1.00 20.00 H
HETATM 48 H5 hem X 1 58.462 15.344 16.090 1.00 20.00 H
HETATM 49 H6 hem X 1 57.809 14.963 17.696 1.00 20.00 H
HETATM 50 H7 hem X 1 56.299 14.725 15.058 1.00 20.00 H
HETATM 51 H8 hem X 1 55.638 14.341 16.657 1.00 20.00 H
HETATM 52 H9 hem X 1 53.130 24.775 17.570 1.00 20.00 H
HETATM 53 H10 hem X 1 59.424 24.528 12.007 1.00 20.00 H
HETATM 54 H11 hem X 1 61.027 17.865 11.728 1.00 20.00 H
HETATM 55 H12 hem X 1 59.939 16.761 12.584 1.00 20.00 H
HETATM 56 H13 hem X 1 62.457 18.061 13.648 1.00 20.00 H
HETATM 57 H14 hem X 1 61.322 17.134 14.649 1.00 20.00 H
HETATM 58 H15 hem X 1 54.456 17.052 19.121 1.00 20.00 H
HETATM 59 H16 hem X 1 54.662 15.588 18.130 1.00 20.00 H
HETATM 60 H17 hem X 1 55.863 15.992 19.380 1.00 20.00 H
HETATM 61 H18 hem X 1 58.989 26.580 11.081 1.00 20.00 H
HETATM 62 H19 hem X 1 58.945 27.155 12.765 1.00 20.00 H
HETATM 63 H20 hem X 1 57.438 26.676 11.949 1.00 20.00 H
HETATM 64 H21 hem X 1 53.083 20.231 19.789 1.00 20.00 H
HETATM 65 H22 hem X 1 52.151 21.741 19.660 1.00 20.00 H
HETATM 66 H23 hem X 1 53.642 21.696 20.631 1.00 20.00 H
HETATM 67 H24 hem X 1 56.425 26.574 15.851 1.00 20.00 H
HETATM 68 H25 hem X 1 56.350 26.983 14.121 1.00 20.00 H
HETATM 69 H26 hem X 1 57.913 27.004 14.973 1.00 20.00 H
HETATM 70 H27 hem X 1 60.367 21.415 11.021 1.00 20.00 H
HETATM 71 H28 hem X 1 61.639 20.255 11.473 1.00 20.00 H
HETATM 72 H29 hem X 1 60.269 19.727 10.466 1.00 20.00 H
HETATM 73 H30 hem X 1 53.271 25.685 19.780 1.00 20.00 H

```
        HETATM   74  H31 hem X   1      54.017  24.192  20.399  1.00 20.00           H
        HETATM   75  H32 hem X   1      52.268  24.243  20.070  1.00 20.00           H
""")
    output.close()


output = open(r"C:\Users\Public\Desktop\T213R_T214I_RED.txt","a")
output.write("DOCKING RESULTS FOR AXR \n")
scorefxn = create_score_function("ligand")
docking = DockMCMProtocol()
docking.set_scorefxn(scorefxn)

params_list = Vector1(["LIGAND_NAME.params"])
res_set = generate_nonstandard_residue_set(params_list)

for i in pose_list:
    v ="C:\Users\Public\\"+ str(i) + ".pdb"
    pose = Pose()
    pose_from_pdb(pose,res_set, str(v))
    job_output = str(i) + "_LIGAND_NAME"
    jd = PyJobDistributor(job_output, 100, scorefxn)
    test_pose = Pose()
    counter = 0
    while not jd.job_complete:
        test_pose.assign(pose)
        counter += 1
        test_pose.pdb_info().name(job_output + '_' + str(counter))
        docking.apply(test_pose)
        test_pose.pdb_info().name(job_output + '_' + str(counter) + '_fa')
        jd.output_decoy(test_pose)

for i in pose_list:
    x = 1
    name ="C:\Users\Public\\"+ str(i) + ".pdb"
```

```
    output.write("*" * 102 + "\n")
    output.write("Docking results of model " + str(name) + "\n")
    for x in range(1,101):
        v = str(i) + "_LIGAND_NAME_" + str(x) + ".pdb"
        pose = Pose()
        pose_from_pdb(pose, res_set, str(v))
        scr = int(scorefxn(pose))
        #if scr <= 0:
        output.write("Docking score " + str(x) + " = %f\r\n" % scr)
        #if scr >= 0:
            #os.remove(r"C:\Users\Public\\" + str(v))

output.close()
```

LIGANDS

AMPLEX®RED

```
HETATM    1  C1  RED X   1      52.429  15.176  13.678  1.00 20.00           C
HETATM    2  C2  RED X   1      53.838  15.783  13.713  1.00 20.00           C
HETATM    3  O1  RED X   1      54.787  15.030  13.845  1.00 20.00           O
HETATM    4  N1  RED X   1      53.995  17.153  13.443  1.00 20.00           N
HETATM    5  C3  RED X   1      52.910  18.042  13.138  1.00 20.00           C
HETATM    6  C4  RED X   1      53.000  18.859  11.989  1.00 20.00           C
HETATM    7  C5  RED X   1      51.933  19.691  11.612  1.00 20.00           C
HETATM    8  C6  RED X   1      50.768  19.728  12.395  1.00 20.00           C
HETATM    9  C7  RED X   1      50.696  18.975  13.581  1.00 20.00           C
HETATM   10  C8  RED X   1      51.770  18.151  13.960  1.00 20.00           C
HETATM   11  O2  RED X   1      54.183  18.903  11.284  1.00 20.00           O
HETATM   12  C9  RED X   1      55.346  18.515  11.916  1.00 20.00           C
HETATM   13  C10 RED X   1      55.271  17.687  13.060  1.00 20.00           C
```

HETATM 14 C11 RED X 1 56.459 17.392 13.762 1.00 20.00 C
HETATM 15 C12 RED X 1 57.698 17.867 13.301 1.00 20.00 C
HETATM 16 C13 RED X 1 57.762 18.659 12.142 1.00 20.00 C
HETATM 17 C14 RED X 1 56.582 18.994 11.456 1.00 20.00 C
HETATM 18 O3 RED X 1 58.962 19.119 11.688 1.00 20.00 O
HETATM 19 H1 RED X 1 59.350 19.713 12.356 1.00 20.00 H
HETATM 20 O4 RED X 1 49.726 20.526 12.022 1.00 20.00 O
HETATM 21 H2 RED X 1 49.975 21.459 12.142 1.00 20.00 H
TER

GUAIACOL

HETATM 1 C1 GGG X 1 55.538 20.323 12.960 1.00 20.00 C
HETATM 2 O1 GGG X 1 54.464 19.802 12.151 1.00 20.00 O
HETATM 3 C2 GGG X 1 54.075 18.523 12.363 1.00 20.00 C
HETATM 4 C3 GGG X 1 54.519 17.695 13.423 1.00 20.00 C
HETATM 5 C4 GGG X 1 54.027 16.401 13.564 1.00 20.00 C
HETATM 6 C5 GGG X 1 53.134 15.899 12.632 1.00 20.00 C
HETATM 7 C6 GGG X 1 52.697 16.692 11.564 1.00 20.00 C
HETATM 8 C7 GGG X 1 53.154 17.964 11.417 1.00 20.00 C
HETATM 9 O2 GGG X 1 52.761 18.802 10.388 1.00 20.00 O
HETATM 10 H1 GGG X 1 55.245 18.072 14.129 1.00 20.00 H
HETATM 11 H2 GGG X 1 54.340 15.790 14.398 1.00 20.00 H
HETATM 12 H3 GGG X 1 52.771 14.887 12.730 1.00 20.00 H
HETATM 13 H4 GGG X 1 51.992 16.290 10.851 1.00 20.00 H
HETATM 14 H5 GGG X 1 55.785 21.332 12.632 1.00 20.00 H
HETATM 15 H6 GGG X 1 55.227 20.346 14.004 1.00 20.00 H
HETATM 16 H7 GGG X 1 56.414 19.683 12.856 1.00 20.00 H
HETATM 17 H8 GGG X 1 53.532 19.070 9.883 1.00 20.00 H
TER

Progesterone

```
HETATM    1  O1  PRS X   1      57.555  21.482  11.357  1.00 20.00           O
HETATM    2  C1  PRS X   1      52.588  15.683  12.426  1.00 20.00           C
HETATM    3  C2  PRS X   1      53.106  14.426  13.164  1.00 20.00           C
HETATM    4  C3  PRS X   1      53.270  16.996  12.886  1.00 20.00           C
HETATM    5  C4  PRS X   1      54.811  16.883  12.648  1.00 20.00           C
HETATM    6  C5  PRS X   1      55.603  18.187  13.047  1.00 20.00           C
HETATM    7  C6  PRS X   1      52.179  13.348  12.535  1.00 20.00           C
HETATM    8  C7  PRS X   1      54.616  14.282  12.844  1.00 20.00           C
HETATM    9  C8  PRS X   1      55.411  15.558  13.232  1.00 20.00           C
HETATM   10  C9  PRS X   1      51.055  15.568  12.484  1.00 20.00           C
HETATM   11  C10 PRS X   1      52.712  18.224  12.133  1.00 20.00           C
HETATM   12  C11 PRS X   1      50.789  14.043  12.422  1.00 20.00           C
HETATM   13  C12 PRS X   1      54.929  19.438  12.456  1.00 20.00           C
HETATM   14  C13 PRS X   1      52.891  14.486  14.713  1.00 20.00           C
HETATM   15  C14 PRS X   1      53.414  19.509  12.598  1.00 20.00           C
HETATM   16  C15 PRS X   1      57.043  18.083  12.459  1.00 20.00           C
HETATM   17  C16 PRS X   1      55.688  18.374  14.589  1.00 20.00           C
HETATM   18  C17 PRS X   1      57.789  19.430  12.436  1.00 20.00           C
HETATM   19  C18 PRS X   1      55.605  20.461  11.903  1.00 20.00           C
HETATM   20  C19 PRS X   1      56.942  20.541  11.845  1.00 20.00           C
HETATM   21  C20 PRS X   1      52.155  11.985  13.254  1.00 20.00           C
HETATM   22  O2  PRS X   1      53.157  11.316  13.444  1.00 20.00           O
HETATM   23  C21 PRS X   1      50.790  11.515  13.760  1.00 20.00           C
TER
```

APPENDIX B

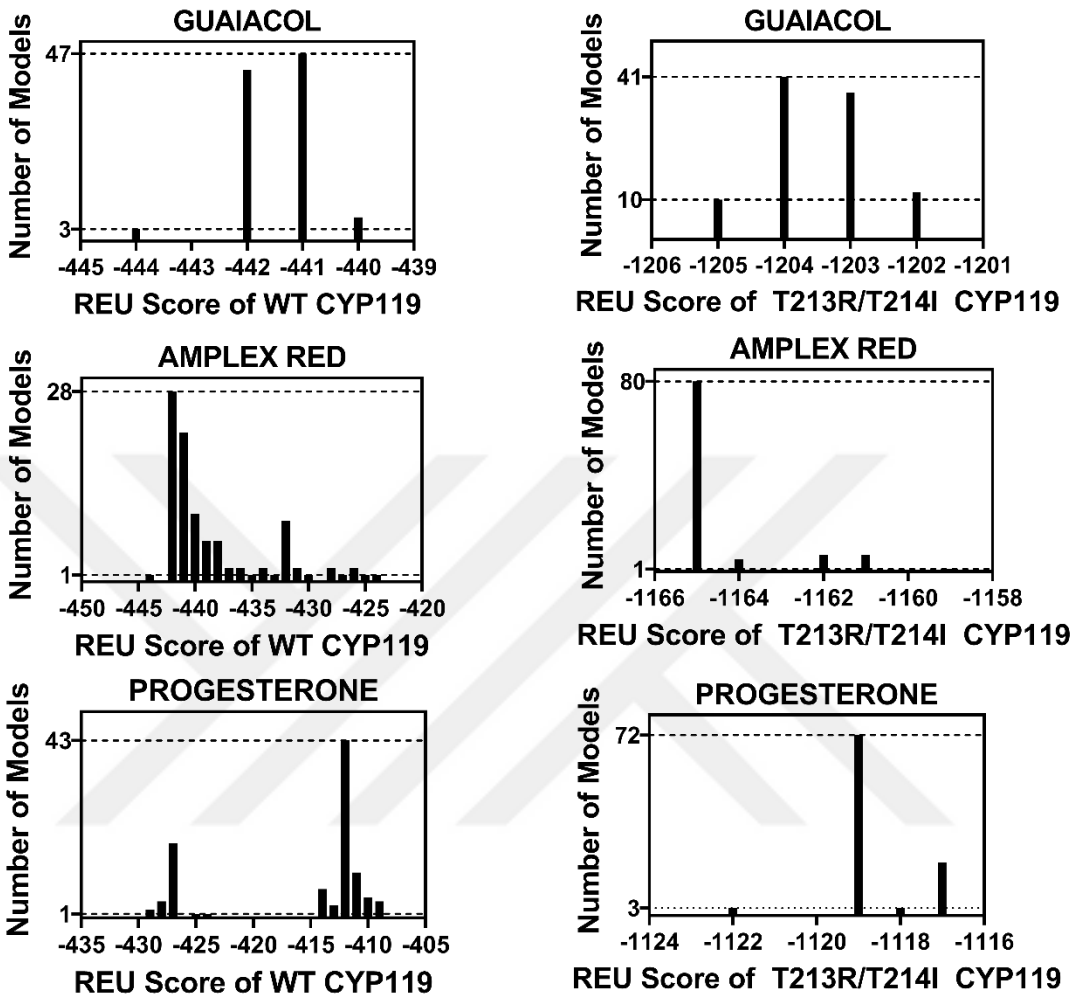

Figure B. 1 REU score distribution graphics of guaiacol, Amplex® Red and progesterone docked T213R/T214I CYP119 and WT CYP119 enzyme. 100 rounds of docking performed for each enzyme.

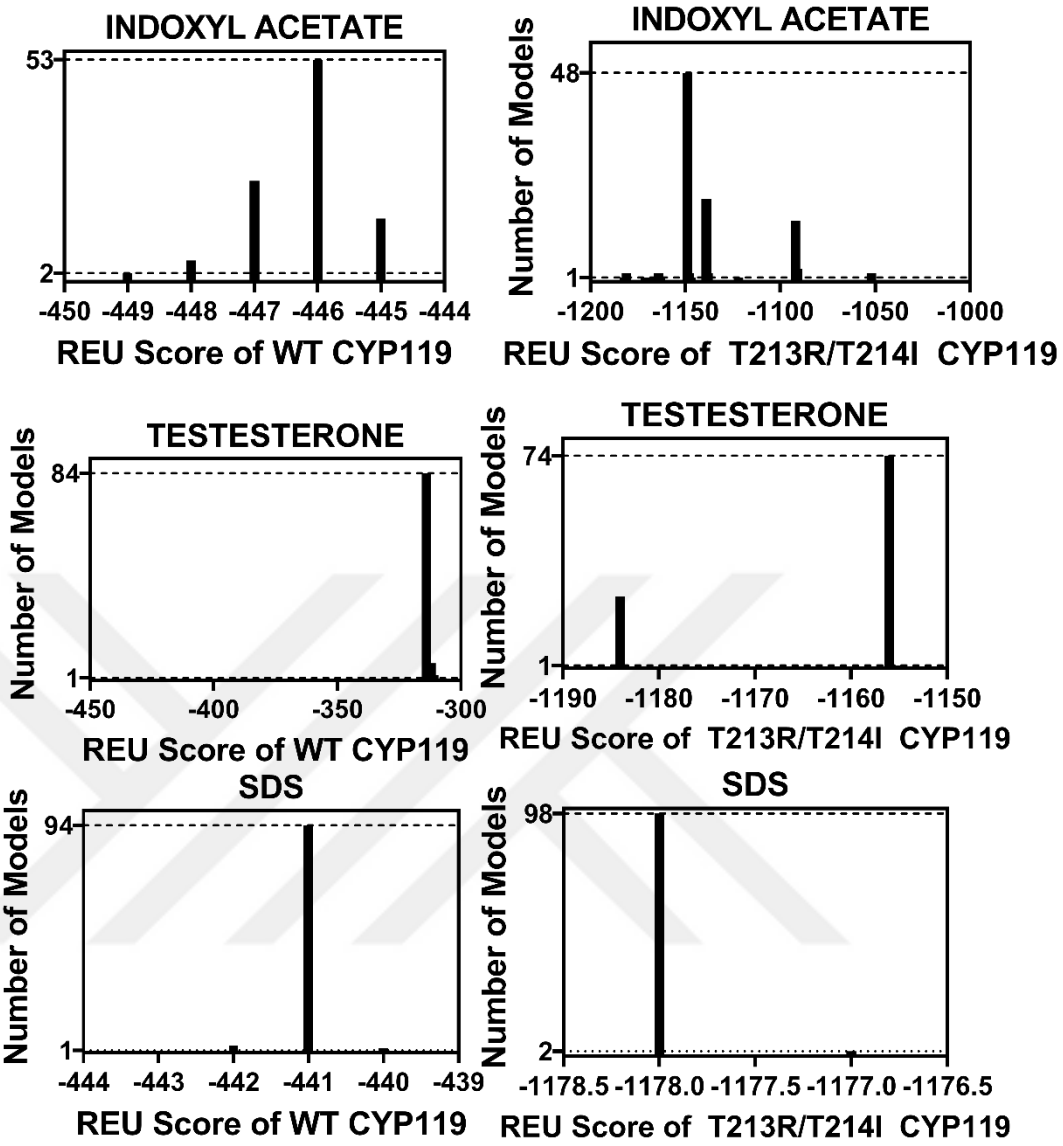

Figure B.2 REU score distribution graphics of indoxyl acetate, testosterone and SDS docked T213R/T214I CYP119 and WT CYP119 enzyme. 100 rounds of docking performed for each enzyme.

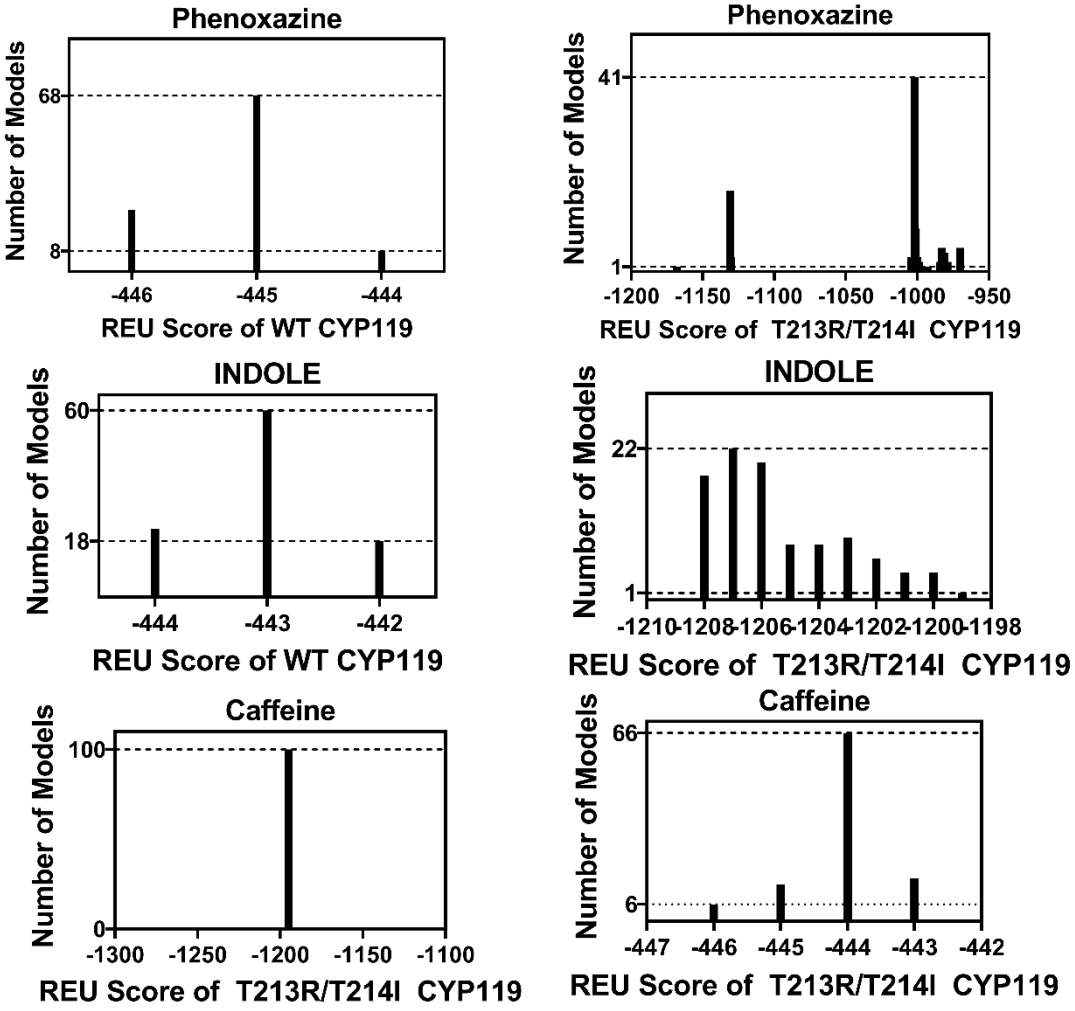

Figure B.3 REU score distribution graphics of docked phenoxazine, indole and caffeine docked T213R/T214I CYP119 and WT CYP119 enzyme. 100 rounds of docking performed for each enzyme.